Polimery w Medycynie

Polymers in Medicine

BIANNUAL ISSN: 0370-0747 e-ISSN: 2451-2699 www.polimery.umed.wroc.pl

2017, Vol. 47, No. 2 (July–December)

Ministry of Science and Higher Education – 9 pts.
Index Copernicus (ICV) – 109.18 pts.

Wroclaw
Medical University

Polimery w Medycynie
Polymers in Medicine

ISSN 0370-0747 (PRINT) ISSN 2451-2699 (ONLINE) www.polimery.umed.wroc.pl

BIANNUAL
2017, Vol. 47, No. 2
(July–December)

"Polymers in Medicine" is an independent, multidisciplinary forum to exchange scientific and clinical information, which publishes original papers (technical, analytical, experimental, clinical), preliminary reports and reviews regarding the use of polymers (natural and synthetic) and biomaterials in different specialties of medicine (biochemistry, clinical medicine, pharmacology, dentistry, implantology), biotechnology and veterinary science.

Address of Editorial Office
Marcinkowskiego 2–6
50-368 Wrocław, Poland
Tel.: +48 71 784 11 33
E-mail: polimery@umed.wroc.pl

Publisher
Wroclaw Medical University
Wybrzeże L. Pasteura 1
50-367 Wrocław, Poland

Online edition is the original version of the journal

Editorial Policy

During the review process, the Editorial Board conforms to the "Uniform Requirements for Manuscripts Submitted to Biomedical Journals: Writing and Editing for Biomedical Publication" approved by the International Committee of Medical Journal Editors (http://www.icmje.org/). Experimental studies must include a statement that the experimental protocol and informed consent procedure were in compliance with the Helsinki Convention and were approved by the ethics committee.

For more information visit the following page: http://www.polimery.umed.wroc.pl

Indexed in: OCLC, WorldCat, PBL, EBSCO, MEDLINE, Index Copernicus

This publication has been co-financed by the Ministry of Science and Higher Education

Typographic design: Monika Kolęda, Piotr Gil
Cover: Monika Kolęda
DTP: Wroclaw Medical University Press
Printing and binding: EXDRUK

Circulation: 47 copies

Polimery w Medycynie
Polymers in Medicine

BIANNUAL 2017, Vol. 47, No. 2 (July–December)

ISSN 0370-0747 (PRINT)
ISSN 2451-2699 (ONLINE)
www.polimery.umed.wroc.pl

Contents

Original papers

Kheri (*Acacia chundra*, family: Mimosaceae) gum: Characterization using analytical, mathematical and pharmaceutical approaches

Rishabha Malviya[1,2,A,B,D–F], Pramod Sharma[1,D], Susheel Dubey[3,F]

[1] Polymer Science Laboratory, Department of Pharmacy, School of Medical & Allied Sciences, Galgotias University, Greator Noida U.P., India
[2] Department of Pharmacy, Uttarkhand Technical University, Dehradun, India
[3] Siddarth Institute of Pharmacy, Dehradun, Uttarkhand, India

A – research concept and design; B – collection and/or assembly of data; C – data analysis and interpretation;
D – writing the article; E – critical revision of the article; F – final approval of the article

Polymers in Medicine, ISSN 0370-0747 (print), ISSN 2451-2699 (online) *Polim Med.* 2017;47(2):65–76

Address for correspondence
Rishabha Malviya
E-mail: rishabhamalviya19@gmail.com

Funding sources
none declared

Conflict of interest
none declared

Acknowledgements
Authors are highly thankful to Prof. D. K. Chauhan from the DD Pant Interdisciplinary Research Laboratory, Department of Botany, University of Allahabad, India, for the authentication of plant materials. Authors would like to thank the Indian Institute of Technology, New Delhi, India, for carrying out mass spectroscopy and NMR study.

Received on March 15, 2017
Reviewed on June 5, 2017
Accepted on August 20, 2017

Abstract

Background. Natural polymers have been used in medical, pharmaceutical, cosmetic and food industry. They should be characterized before their possible applications in different industries.

Objectives. The objective of this study was to characterize Kheri (*Acacia chundra*, family: Mimosaceae) gum using analytical, mathematical and pharmaceutical approaches.

Material and methods. Crude Kheri gum (KG) was purified using distilled water as a solvent and ethanol as a precipitating agent. KG was characterized in terms of phytochemical screening, micromeritic properties, microbial load, ash value, rheological behavior, solid state ^{1}H nuclear magnetic resonance (NMR), mass spectra and Fourier-transform infrared spectroscopy (FTIR) studies for their possible applications in food, cosmetics and pharmaceutical industry.

Results. Studies show that KG contains carbohydrates, while protein, fat, volatile oils, alkaloids and glycosides are absent. 1% aqueous solution of polysaccharide showed 25.58×10^3 kJ/kg activation energy and 1.39 Reynold's number. Viscosity average molecular weight of purified gum was found 1.73×10^5 D. Thermodynamic parameters, i.e., change in enthalpy ΔHv and change in enthalpy ΔHv, were found to be 12.26×10^3 kJ/mol and 24.47 kJ/mol, respectively. Mathematical approach also determined the rod shaped conformation of KG in aqueous solution. IR spectroscopic study shows the presence of free (COO–) and esterified (COO–R) carboxylic acid, ether (C–O stretching), galacturonic acid and mannose in polysaccharide ^{1}H NMR study predicts presence of tetrahydropyran hydrogen in molecule. Furthermore, KG was also characterized as a suspending agent using paracetamol as a model drug. Flow rate, pH, particle size and settling behavior of suspensions were evaluated. Initial particle size of dispersed phase particles does not change significantly after 45 days.

Conclusions. From the findings of the research it can be concluded that KG can be used as an excipient in cosmaceuticals and pharmaceuticals and its characteristic rheological behavior may attract rheologists.

Key words: characterization, suspending agent, rheological behavior, Kheri gum, spectra

DOI
10.17219/pim/76515

Introduction

Water-soluble gums are also known as hydrocolloids. Hydrocolloids have been used in pharmaceutical, agriculture, food and cosmetic industry depending on their characteristics, rheological and molecular behavior. Gums have been successfully used for the treatment of industrial effluents. They are generally used as a gelling agent, a thickening agent, an emulsifying agent and a suspending agent due to their long, branched, chain structure. The chain length, ring structure and molecular weight determine the interaction to fluid, hence rheological behavior.[1] Gums are obtained as exudates mainly from fruit and the trunk of plants after injury or incision, or after microbial invasion. Gum exudates are nodule or ribbon-shaped and act as a protective measure against a microbial attack. Gums are either a metabolic product of a plant or produced to conteract undesirable conditions.

Kheri gum (KG) (*Acacia chundra*, family: Mimosaceae) is widely distributed in the Gujarat, Maharashtra and Rajasthan regions of India. The trees have medicinal properties and are used as a source of timber and fodder. Gum obtained from the tree is a good substitute for acacia gum.[2] The rheological behavior of the polymeric solution has been a topic of great interest among rheologists for their possible use in food, cosmetics and the pharmaceutical industry. Significant advances have been made in the characterization of the polymer, and in this paper green technology and mathematical approaches were used to characterize the rheological behavior of the polymer. The objective of the present research work was to characterize KG for their possible pharmaceutical and biomedical applications.

Material and methods

Crude gum was purchased from a local shop in New Delhi, India (Tyagi Herbal Products, Khari Bawali, Chadani Chowk). The gum was authenticated by Professor D. K. Chauhan (Department of Botany, University of Allahabad, India).

Purification of polysaccharide

Crude gum was dissolved in a sufficient amount of purified water and heated up to 40°C. After 2 h, the gum solution was filtered through a double folds muslin cloth to remove un-dissolved portion. The gum was precipitated by using ethyl alcohol and dried in an oven at 40°C. Further, the gum was powdered, passed through 60# (0.25 mm) sieve and stored in an airtight polypropylene jars under desiccated condition.

Characterization of neutral ginseng polysaccharides

Phytochemical screening of gum

As described by authors elsewhere, tests for carbohydrates, protein, fats, organic acids, glycosides, tannins and alkaloids were carried out for the phytochemical characterization of purified KG.[3]

Organoleptic characteristics of gum

Organoleptic properties are directly characterized using sense organs, which is why they are called organoleptic properties. Color, odor, taste, fracture and texture were evaluated to characterize the gum.[4] A protocol was prepared to evaluate the taste and odor of KG. A total of 6 volunteers were selected for the study, with an age group of 18 to 35 years, out of which 3 were males and 3 females. Informed consent was obtained from volunteers. Volunteers were excluded if they had any of the following diseases or disorders:

- disease which affects taste perception, such as a thyroid disorder, diabetes mellitus and Cushing's syndrome, etc.;
- internal disorders, such as renal and hepatic disorders;
- middle ear infections;
- pregnancy, smoking behaviour, alcoholic, use of other medication, impaired perception towards taste and allergic reactions to artificial sweeteners.

To rate the taste of KG; 0.32M NaCl, 1mM quinine, 1M NaCl and 1% w/v solution of KG were painted over the tip of the tongue, sipped and swished in the mouth for 15 s, and then spat out. Volunteers rated the intensity of the taste on GLMS. Standard numerical value of taste for 1mM quinine, 1M NaCl and 0.32M NaCl was 10, 7 and 5, respectively.

To determine the odor of KG, the smell of natural gas, smoke, orange and chocolate was used for identification. Volunteers who were not able to identify the odor were excluded from the study. Laboratory temperature was maintained at 25–27°C for the comfort of the volunteers. Odor intensity and intensity level were presented in Table 1.

Table 1. Intensity level value for odor intensity

Scale number	Odor intensity	Intensity level
1	extremely strong	A
2	very strong	B
3	strong	C
4	distinct	D
5	weak	E
6	very weak	F
7	not perceptive	G

Solubility profile and pH

As described in a previous publication, 1 part of dry powdered polysaccharide was shaken with different solvents and the solubility was determined. One percent w/v solution of powdered gum was prepared and the pH was determined.[4]

Particle size analysis

Particle size of powdered gum sample was analyzed using optical microscopy – (Globus, Ph/L/16/02) (Rajas, Noida, Uttar Pradesh, India). Magnification value of microscope was calculated using overlapping point of eye piece and stage micrometer. In this measurement, 50 particles in 5 different fields were examined.

Limit test for heavy metals

Limit test for heavy metals (Pb) and arsenic were carried out as per procedure mentioned in "Indian Pharmacopoeia".[5]

Qualitative test for Cl^- and SO_4^{2-}

Qualitative tests for Cl^- and SO_4^{2-} were examined using the method given in "Indian Pharmacopoeia".[5]

Determination of microbial load

Microbial load was determined to detect the presence of viable forms of microbes (bacteria, fungi and yeast). The method is based on the principle that in a nutritive medium, microbes grow and their presence can be detected by turbidity in the clear solution. Microbial load was determined as per Indian Pharmacopoeia.[5] Values were shown as an average of triplicate studies with standard deviation.

Determination of total ash, total soluble ash, acid insoluble ash and sulphated ash

Total ash and related parameters have been used to characterize natural polymers. Standard AOAC method was used to estimate ash value of neutral ginseng polysaccharides (NGP).[6] One gram of polysaccharide was taken and transferred to a pre-ignited and pre-weighed crucible and the total weight of the crucible with sample was noted. Further, the gum crucible was transferred into a furnace. The ignition temperature was maintained at 550°C for 24 h. Ash value was calculated using equation 1. Afterwards, the recovered ash was used to calculate the total soluble ash using equation 2:

$$\text{total ash (\%)} = \frac{\text{actual weight of ash}}{\text{original weight of sample}} \times 100 \quad (1),$$

$$\text{total soluble ash} = \text{total ash (\%)} - \text{total insoluble ash (\%)} \quad (2).$$

Acid insoluble ash and sulphated ash were calculated after the ash was treated with HCl and H_2SO_4,respectively. Different ash values were shown as an average of triplicate studies with standard deviation.

Viscosity measurement

To determine viscosity 1% w/v solution of polysaccharide was prepared in purified water. Relative viscosity was determined using Ostwald's capillary viscometer (Rajas, Noida, Uttar Pradesh, India).

The effect of shear rates on the viscosity of the polymer was measured using Brookfield viscometer (National Analytical Corporation, Maharashtra, India). Viscosity of the polymer was measured at shear rates from 0.1 to 2.0 s^{-1} at 27°C. Relative viscosity (η_{rel}), specific viscosity (η_{sp}) and reduced viscosity (η_{red}) was calculated using Equations 3, 4 and 5 at 27°C, respectively:

$$\eta_{rel} = \frac{\eta}{\eta_0} \quad (3),$$

$$\eta_{sp} = \eta_{rel}^{-1} \quad (4),$$

$$\eta_{red} = \frac{\eta_{sp}}{C} \quad (5),$$

where η is intrinsic viscosity and C is concentration of polymer.

Effect of electrolytes and surfactant on the viscosity of polysaccharide

The effect of electrolytes (calcium chloride, sodium chloride, and potassium chloride), surfactant (sodium lauryl sulphate) and citric acid on the viscosity of 1% KG solution was determined. One percent solution of electrolytes, surfactant and citric acid were individually prepared and 5 mL of the prepared solutions were added to 100 mL 1% solution of KG. Then, the viscosities of individual samples were determined at 27°C.

Effect of temperature on the viscosity and determination of thermodynamic parameters

Temperature changes the viscosity of liquid. The viscosity of liquid decreases with the increase in temperature. The effect of temperature on the viscosity was shown as a graph of viscosity vs the centigrade temperature.

The effect of temperature on the viscosity can be shown by the Arrhenius equation (equation 6):

$$\eta = A \exp \frac{E}{RT} \quad (6),$$

where A is a constant for a liquid. Activation energy for viscous flow can be calculated from the slope of the graph

between the logarithm of viscosity and reciprocal of the Kelvin temperature. Ideally, the plot between ln η and $1/T$ should be linear and the value of the slope is equal to E/R.

Osborne Reynolds also describes an exponential equation to describe the effect of temperature on the viscosity as per equation 7:

$$\eta = R \exp [\alpha T] \quad (7),$$

where R is Reynolds number and α is a constant. Reynolds number and α was calculated from the graph between ln viscosity and temperature.

Thermodynamic parameters such as change in enthalpy ΔHv and change in entropy ΔSv of polymeric solution can be calculated using Frenkel-Eyring equation 8:

$$\ln [\frac{\eta}{T}] = (\ln A - \frac{\Delta Sv}{R}) + \frac{\Delta Hv}{RT} \quad (8).$$

From equation 8, the graph can be plotted between ln $[\eta/T]$ and $1/T$ having slope and intercept $\Delta Hv/R$ and ln $A - \Delta Sv$ respectively.[7]

Determination of intrinsic viscosity

Hydrodynamic volume occupied by a single polymer molecule is measured in terms of intrinsic viscosity. Hydrodynamic volume depends upon the size and conformation of the polymeric chain. Generally, intrinsic viscosity is determined at a low polymer concentration. Intrinsic viscosity is measured by calculating specific viscosity at various concentrations at a fixed temperature and shear rate. Intrinsic viscosity can be determined using the Huggins equation (equation 9):

$$\frac{\eta_{sp}}{C} = [\eta] + K[\eta]^2 C \quad (9),$$

η_{sp}/C is known as reduced viscosity. It is clear from equation 8 that a graph between reduced viscosity and concentration should be linear with the slope showing the value of $K[\eta]^2$ and intercept $[\eta]$. Huggins constant K can be calculated from the value of slope and $[\eta]$.

Kraemer equation (equation 10) can be used to analyze intrinsic viscosity:

$$\ln (\frac{\eta_{sp}}{T}) = [\eta] + K_0[\eta]^2 C \quad (10),$$

where K_0 is Kraemer constant. A graph between ln (η_{sp}/C) and concentration C should be a straight line with the slope showing the value of $K_0[\eta]^2$ and intercept $[\eta]$. Huggins constant K_0 can be calculated from the value of the slope and $[\eta]$.

Tanglertpaibul and Rao derived 3 equations (equations 11, 12 and 13) for the determination of the intrinsic viscosity of a polymeric solution[8]:

$$\eta_{rel} = 1 + [\eta]C \quad (11),$$

$[\eta]$ is the slope of the graph plotted between η_{rel} and C.

$$\eta_{rel} = e^{[\eta]C} \quad (12),$$

$[\eta]$ is the slope of the graph plotted between ln η_{rel} and C.

$$\eta_{rel} = 1/(1 - [\eta]C) \quad (13),$$

$[\eta]$ is the slope of the graph plotted between $1/(1 - \eta_{rel})$ and C.

Molecular conformation, polymer interaction and coil overlap parameter

Generally, power law equation 14 is used to study the molecular conformation, polymer interaction and coil overlap parameter:

$$\eta_{sp} = {}_aC^b \quad (14).$$

Mathematically, equation 14 can be shown as equation 15:

$$\ln \eta_{sp} = \ln a + b \ln C \quad (15).$$

The value of constant b is important to determine the conformational behavior of a polymer in dilute solutions.

Determination of molecular weight

Concentration dependency of viscosity can be represented by equation 8, where K is known as Huggins constant. It was found that when the polymer is dispersed in a good solvent, the value of K is near 0.35 and relatively more value is observed when the polymer is dispersed in a poor solvent. Constant α is known as "shape parameter" and is related to the conformation of the polymer in a particular solvent. The value of α is 0 for a nonsolvent (in which the polymer precipitates). In a good solvent, the value of α varies from 0.5 to 1. Viscosity-average molecular weight (M) can be estimated from intrinsic viscosity using Mark Houwink equation (equation 16):

$$[\eta] = k M^{\alpha} \quad (16),$$

where $\alpha = 0.732$ and $k = 3.8 \times 10^{-4}$,
where 2 constants are characteristics of each solute-solvent system. For most of the polysaccharides, the value of M shows a weight average value, in spite of the number average value.[9]

Determination of surface tension

One percent w/v solution of the gum was prepared using distilled water, and surface tension was determined using stalagmometer (Rajas, Noida, Uttar Pradesh, India). Surface tension was shown as the average of triplicate studies with standard deviation.

Foaming capacity and foam stability

To measure foaming capacity, 1 g of polysaccharide was mixed with 100 mL of distilled water (q.s.). The gum was dissolved using a high-speed blender (at 5000 rpm) and the prepared solution was immediately transferred into a 250 mL measuring cylinder. Foaming capacity (%) and foam stability (%) were calculated using equation 17 and equation 18, respectively. Foam stability was measured after 15 min. Foaming capacity and foam stability was determined 3 times and the results were shown as the average of triplicate studies with standard deviation.

$$\text{foam capacity (\%)} = \frac{\text{foam volume after blending} - \text{foam volume before blending}}{\text{foam volume before blending}} \times 100 \quad (17),$$

$$\text{foam capacity (\%)} = \frac{\text{foam volume after time } (t)}{\text{initial foam volume}} \times 100 \quad (18).$$

Swelling index and water holding capacity

As described in a previous publication, swelling index (%) of the polymer was calculated. To measure water holding capacity, 1 gm of polysaccharide was added in 25 mL of distilled water and kept for 12 h, which was followed by centrifugation at 5000 × g for 30 min.[3] Supernatant was removed and the water-holding capacity was calculated using equation 19. The results were shown as an average of triplicate studies with standard deviation.

$$\text{water holding capacity (\%)} = \frac{\text{weigh of wet sample} - \text{weight of dry sample}}{\text{weight of dry sample}} \quad (19).$$

Micrometric properties and flow behavior of polymer

Micrometric properties such as bulk density, tapped density, bulkiness, Carr's Index, Hausner's ratio and angle of repose of gum was performed 3 times as described in previous publications.[3]

Surface morphology

Surface morphology of powdered gum was studied using scanning electron microscopy (SEM). SEM study was performed at the Department of Textile Engineering, Indian Institute of Technology New Delhi, India.

Fourier transform infrared spectroscopy

Fourier-transform infrared spectroscopy (FTIR) analysis was performed at Central Instrument Facilities, School of Medical and Allied Sciences, Galgotias University, Greater Noida, India. Dried powdered gum sample was put on the analyzer plate of Bruker ATR equipment (Alpha, ECD-ATR) (Bruker Optics K.K. Yokohama, Japan). The obtained spectra was recorded and interpreted to analyze functional groups present in the polysaccharide.

Nuclear magnetic resonance (^{1}H NMR)

Nuclear magnetic resonance (NMR) spectra were recorded using dimethyl sulfoxide (DMSO) as a solvent at the Indian Institute of Technology, New Delhi, India.

Mass spectroscopy study

Mass spectrometry is an important tool used to analyze the structure of a polymer. Mass spectra's are used to elucidate the structural characterization with linkage, bond type and configuration of polysaccharides. Mass spectral study was performed at the Indian Institute of Technology, New Delhi, India, using matrix assisted laser desorption/tonization – time of flight (MALDI-TOF) mass spectroscopy.

Formulation of suspension

Paracetamol suspensions of NGP were prepared and evaluated for possible suspending properties of polysaccharide. In this study, NGP (0.5, 0.75, 1.25, 1.5 and 1.75% w/v) was used as a suspending agent, benzoic acid (1%) as preservative and paracetamol as model drug. Suspensions were prepared by triturating gum and drug simultaneously, followed by the addition of preservatives.

Organoleptic characteristics and pH of suspension

Organoleptic properties, such as color, odor and taste of prepared formulations, were analyzed by direct perception. Organoleptic properties are characteristics that can be observed by sense organs. Eyes were used to observe color while nasal cavity to detect odor. The taste of formulations was observed by taking 0.1 mL of the formulation on the tongue as determined for KG.

The pH of the formulations was measured by a laboratory pH meter – Decibel Digital Technologies, DB-1002 (Philips India Limited, Chandigarh, India).

Rheological characteristics of suspension

The time required for each suspension sample to flow through a 10 mL pipette was determined and the apparent viscosity was calculated using equation 20:

$$\text{flow rate} = \frac{\text{volume of pipette [mL]}}{\text{flow time [s]}} \quad (20).$$

Viscosity of samples was also determined at 27°C using Brookfield viscometer at 25 RPM.[10]

Settling behavior of suspension

Prepared suspensions were transferred into a graduated cylinder and the sediment volume was observed after a predetermined time (at every 1 h for 7 h and then every 24 h for 7 days). The rate of settling (F) was calculated using equation 21:

$$F = \frac{V_u}{V_o} \quad (21),$$

where V_u is the volume of sediment and V_o is the total volume of suspension.

Redispersion time of the prepared formulation was measured (after 45 days) by inverting the formulation and additional required time for uniform distribution of disperse phase was determined.

Particle size analysis was also carried out for dispersed phase to study any crystal growth or particles aggregation.

Results and discussion

The content of any polysaccharide may be changed significantly, even in small variations of environmental condition and soil characteristics. After the study was conducted, crude gum sample was stored as a reference sample for future prospectives. Thin-layer chromatography (TLC) report, infrared (IR) spectra, Mass spectra and NMR report was kept with sample for referencing purpose. In the future, any researcher would be able to differentiate their own KG from the studied KG based on reference data. On performing chemical test, it was found that carbohydrate was present in KG, while fat, tannin, glycoside, alkaloids, volatile oil, proteins and organic acids were absent. The gum was whitish brown, odorless and characteristic in taste, with rough fracture and irregular texture.

All the volunteers were able to rate the brightness of light, so no one was excluded from the study. On GLMS scale, the value of taste for KG can be denoted as "0".

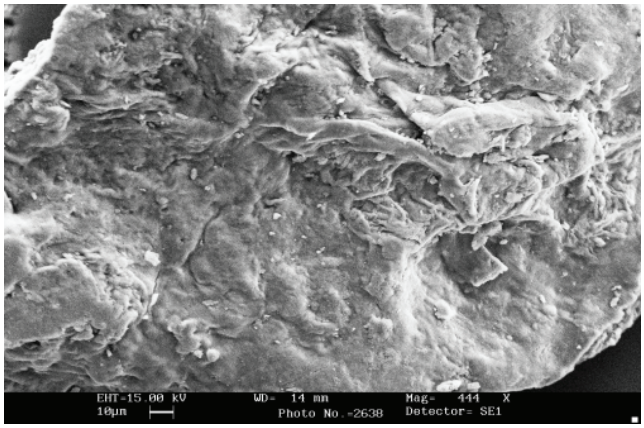

Fig. 1. SEM photograph of Kheri gum polysaccharide

All the volunteers were able to identify the odor of natural gas, smoke, orange and chocolate, so no one was excluded from the study. On the intensity scale, the intensity level of KG can be marked as "G".

Powdered gum was found to be soluble in both cool water (25°C) as well as warm water (40°C). Polysaccharide was insoluble in benzene, n-hexane, diethyl ether, chloroform, cyclohexane, acetone, ethanol and methanol. Kheri gum can be used as pharmaceutical excipient in dermal as well as oral formulation without any irritant effect as the pH of 1% of the solution was found to be 6.7 ±0.0.67. This shows the neutral nature of the polymer. The particles size of the powdered gum was ranged from 41.32 to 77.13 µm with mean size of 61.2 µm.

Analysis determined that heavy metals (lead and arsenic) and Cl^- and SO_4^{2-} were absent in powdered gum. The value of microbial load was found within in the pharmacopoeial limit. It was established at 83 ±10.11 CFU/g and 104 ±7.67 CFU/g for bacteria and fungi, respectively. This might be due to the use of alcohol during the precipitation process.

Total ash, water soluble ash, acid insoluble ash and sulphated ash of polysaccharide was found to be 12.5 ±0.13%, 7.23 ±0.18%, 12.44 ±0.21% and 11.5 ±0.33%, respectively. The value of ash content indicates the proportion of insoluble materials present in gum.

Viscosities of calcium chloride, sodium chloride, potassium chloride, sodium lauryl sulphate and citric acid containing solutions were found to be 1.055; 0.798; 0.790; 0.814 and 0.92, respectively. The results showed that calcium chloride containing solution showed a relatively high viscosity, which may be due to the presence of divalent Ca^{2+} ions that further causes gel formation with polysaccharide. Sodium ions and potassium ions also form monovalent salts with polysaccharide. The solubility of potassium salts are higher than the sodium salts of polysaccharide, which is why potassium salts containing solutions showed less viscosity than sodium containing salts. In the presence of citric acid, the solubility of the polymer decreases and shows a relatively higher viscosity as compared to sodium and potassium salts containing solutions.

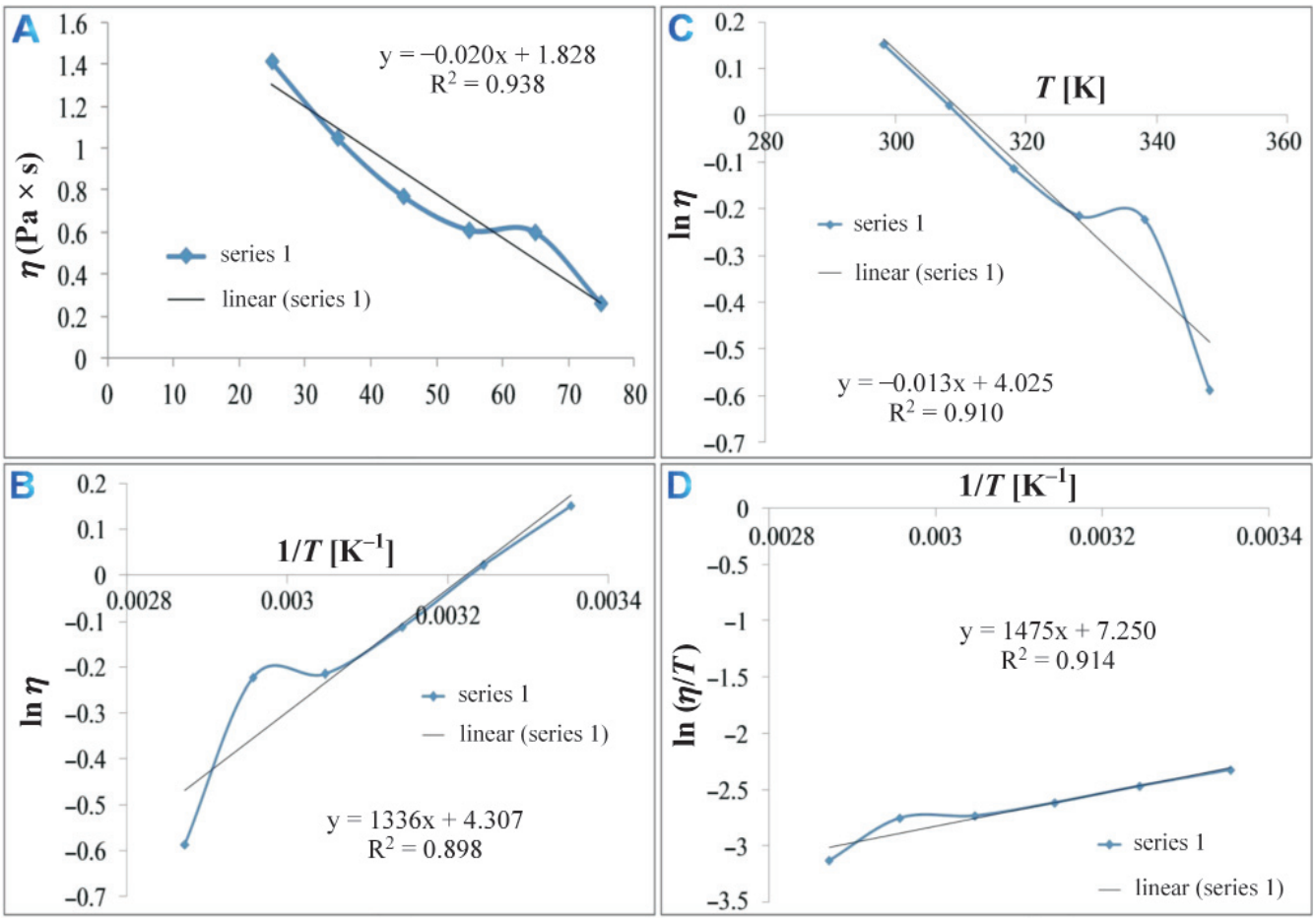

Fig. 2. A – effect of temperature on viscosity; B – determination of activation energy using Arrhenius equation (6); C – effect of temperature on the viscosity as per Reynold's equation (7); D – determination of thermodynamic parameters using Frenkel-Eyring equation (8)

To determine the effect of temperature on viscosity, a Brookfield viscometer was used. Viscosity is the measure of how easily molecules flow with respect to another molecule. It can be concluded from the Fig. 2A that as the temperature increases, viscosity of polymeric solution decreases. Temperature increases the kinetic energy of molecules and thus promotes the easiness of flow. During literature survey, it was found that the plot of the logarithm of viscosity, ln (η), against the reciprocal of absolute temperature ($1/T$) for solutions is almost linear and activation energy can be calculated from the slope of the plot. This process is known as non-isothermal kinetic model for determination of activation energy. In case of non-linear plot, activation energy can be calculated for 2 continuous temperatures.

Activation energy can be estimated from the slope (equation 22) of Arrhenius equation (equation 6):

$$\text{slope} = \frac{E}{2.303R} \qquad (22),$$

where R is gas constant and value of R is 8.314 kJ kg^{-1} mol^{-1} K^{-1}. Activation energy E for 1% w/v solution of the polymer at 27°C was found to be 25.58 × 10^3 kJ kg^{-1}.

This energy predicts polymer solutions sensitivity towards temperature. The value of E is considered as an energy barrier for the gelation of the polymeric solution at a particular temperature.[11] The intercept of the graph (Fig. 2B) was used to calculate Arrhenius constant and it was found to be 4.31. The value of linearity (0.898) for semilog plot of viscosity with the inverse of absolute temperature predicts the linear dependency of activation energy with different temperatures. Activation energy for a polymeric solution depends upon hydrogen bonding, configurational changes and hydrophobic interactions.

The effect of temperature on the viscosity of a polymer, as per Reynold's equation, was shown in Fig. 2C. A graph was used to calculate Reynold's number and constant α. The value of Reynold's number and constant α was found to be 1.39 and 0.03, respectively.

For the estimation of thermodynamic parameters of NGP solution, a graph was plotted based on Frenkel-Eyring equation (8) and shown in Fig. 2D. As per the Fig. 2D, the value of the slope was found to be 1475 and so a change in enthalpy ΔHv was 12.26 10^3 kJ/mol. In polymeric conformation, an energy barrier exists, which is measured in terms of the amount of energy required by molecules to jump from one equilibrium position to another. Mathematically, the energy barrier is measured by a change in enthalpy ΔHv.

The value of pre-exponential factor A was calculated by the intercept of the Fig. 1B based on Arrhenius equation ($\ln A = -4.307$). The value of pre-exponential factor A was further used to calculate a change in entropy ΔSv using Frenkel-Eyring equation. The value of ΔSv was calculated and found to be 24.47 kJ/mol. The positive value of ΔSv indicated coiled conformation of the polymer in dilute solutions.[12] The solubility of the polymer having coiled conformation can be improved by heating, which facilitates the unfolding of a polymer chain. Furthermore, after dissolution, the polymeric chains maintain coiled conformation, unless the chain is rigid. Positive value of ΔSv is due to a greater number of conformation of the polymer in dilute solution. Generally, entropy of mixing shows a lower value for dilute solutions and is governed by a very short ranged interactions, i.e. vander Walls force, hydrogen bonding and dipole–dipole. It was also found that the interaction between solvent–solvent, polymer–polymer and solvent–polymer changes significantly during mixing of polymer due to conformational changes in polymeric chain.

Huggins, Kraemer and Tanglertpaibul and Rao techniques are classical methods for the estimation of intrinsic viscosity and are based on linear graphical extrapolation of the experimental data.[13]

Intrinsic viscosity was found to be 2.06 c-poise (Huggins equation) (Fig. 3A), 0.997 c-poise (Kraemer equation) (Fig. 3B), 0.623 cPoise (Tanglertpaibul and Rao equation 11), 0.176 cPpoise (Tanglertpaibul and Rao equation 12) and 2.618 c-poise (Tanglertpaibul and Rao equation 13).

Intrinsic viscosity depends upon molecular weight, conformational size and shape and specific volume. Interaction and conformation of polymer within solvent also depends upon concentration of polymer at fixed volume of solvent. Effective volume fraction of polymer in solution is expressed in terms of "space occupancy" or "coil overlap", which is a product of a concentration and intrinsic viscosity ($[\eta].c$). As per equation 15, the plot between $\ln \eta_{sp}$ and $\ln C$ was found a linear slope and an intercept equal to b and ln, respectively (not shown here). The value of R^2 was found to be 0.959, and elicits good linearity. The value of b was found to be 0.532 and is an important parameter for determining the conformation of polysaccharide. The value of constant b is below 1; hence, it elicits the presence of rod like conformation of gum.

Viscosity average molecular weight of KG polysaccharide was found to be 1.73×10^5 D using intrinsic viscosity data from Huggins equation 9. The surface tension of 1% w/v solutions of polysaccharide was found to be 136.43 ±3.13 dyn/cm^2. Wetting and spreading properties was determined by the surface tension of any polymer. The surface tension also influences the effect of biological fluid on the pharmaceutical formulation made up of a respective polymer. The lower surface tension promotes better interaction and penetration of biological fluid within delivery system.

Foaming ability is an important parameter characterizing gum. Foam capacity and foam stability of 1% w/v solution of KG was found to be 58 ±1.37% and 63 ±1.09%, respectively. Foam is generally produced by the turbulent flow, which causes the entrapment of air bubbles in liquid. Stability of foam depends upon the difference in density between the gaseous phase and the liquid medium. The use of surfactant decreases surface energy between 2 phases and improves the stability of the foam system. Polysaccharides are not used to prepare foam, but their presence improves the stability of other foams due to their 3-dimensional polymeric structure.

The swelling index of polysaccharide was found to be 70 ±4.33%, while the water-holding capacity of the polymer was 95 ±5.67 g water/g of dry powdered polysaccharide. The value obtained after the study elicits the fact that the polymer has a good attraction towards water, so KG is hydrophilic in nature. The bulk density and tapped

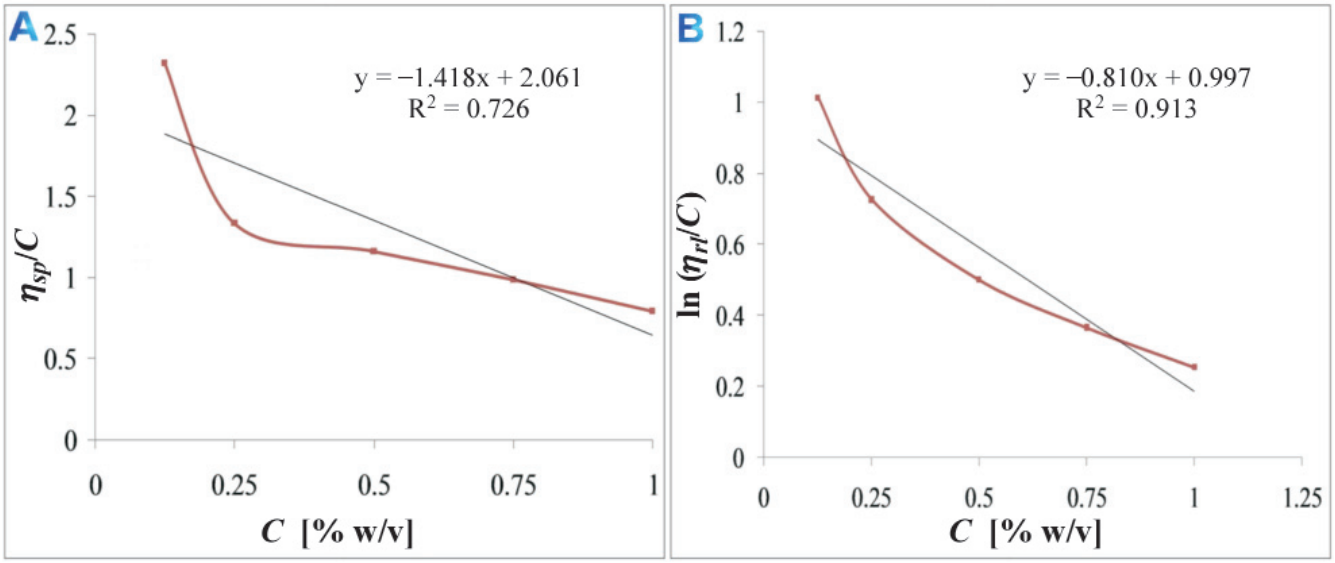

Fig. 3. Determination of intrinsic viscosity (A) using Huggins equation (9) and (B) Kraemer equation (10)

density are used to characterize compactation properties and packing arrangements of polymer. KG was characterized for its micromertitic properties such as bulk density (0.71 ±0.16 g/mL), tapped density (0.83 ±0.04 mg/mL), Carr's index (14.28 ±0.19), Hausner's ratio (1.16 ±0.07) and angle of repose (19.8 ±0.53°). The bulkiness value is used to describe 'heaviness' of powder and was 1.60 ±0.04 mL/mg. The angle of repose is used to characterize the flow behavior of the polymer for better industrial applications. In the present study, the value of the angle of repose was 19.8 ±0.53°, which indicates "good" to "passable" flow behavior of KG. The value of tapped density was found to be more than the bulk density, which indicates the amount of entrapped air and packing arrangement of particles.

Infrared spectroscopy is used to determine the identity of the compound (Fig. 4). The region below wave number 1500 cm^{-1} shows much absorption caused as a result of bending and stretching vibrations. In this region, the numbers of bending vibrations are more than the number of stretching vibrations and are known as the finger print region. Stretching vibrations arise due to C–C, C–O and C–N bonds. The bonds in the region 1149–1018 cm^{-1} were corresponding to C–O–C and C–O–H of glycosidic linkage. Absorption bands around 1618 and 1430 cm^{-1} were due to characteristic peaks of carboxylate group of galactoronic acid residue. Ethers show only one characteristics band in the region 1300–1050 cm^{-1}. The peak at 1242.12 cm^{-1} shows C–O–C absorption spectrum of ether (C–O stretching). The peak at 1421.97 cm^{-1} represents the symmetric stretching of carboxylic group of uronic acid. Hence, uronic acid may be present in polysaccharide. The peak at 1620.15 cm^{-1} could be due to the stretching of mannose. The peak at 1742.78 cm^{-1} shows the characteristic peaks of C=O stretching of saturated esters. The peak at 3561.66 cm^{-1} may arise due to intramolecular hydrogen bonded O–H group. Carbonyl absorption bands showing the peak at 1620 and 1740 cm^{-1} were due to free (COO–) and esterified (COO–R) carboxyl groups, respectively.

Mass spectral analysis provides information about internal cleavage, sequence and branching. Interpretations of spectra provide knowledge about linkage side of monomer to form polymer. A mass spectrum of polysaccharide is shown in Fig. 5. Generally, carbohydrates show initial cleavage of glycosidic bond (–C–O– bond). Different literatures described fragmentation pattern through ring cleavages. After ring cleavage, both ions retain the charge of the molecular species.[14]

Nuclear magnetic resonance uses ^{1}H, ^{13}C, ^{15}N and ^{31}P as tracer atoms for spatial information about the structure. Nuclear magnetic resonance study is widely used to elucidate the conformational aspects of polysaccharide structure. It was also found during literature survey that NMR study can be used to elicit the relationship between spatial structure of molecules and their biological activity. In this study, ^{1}H NMR spectra was used to characterize polysaccharide. Polysaccharide sample was analyzed and a spectrum was shown in Fig. 5, shift values were shown

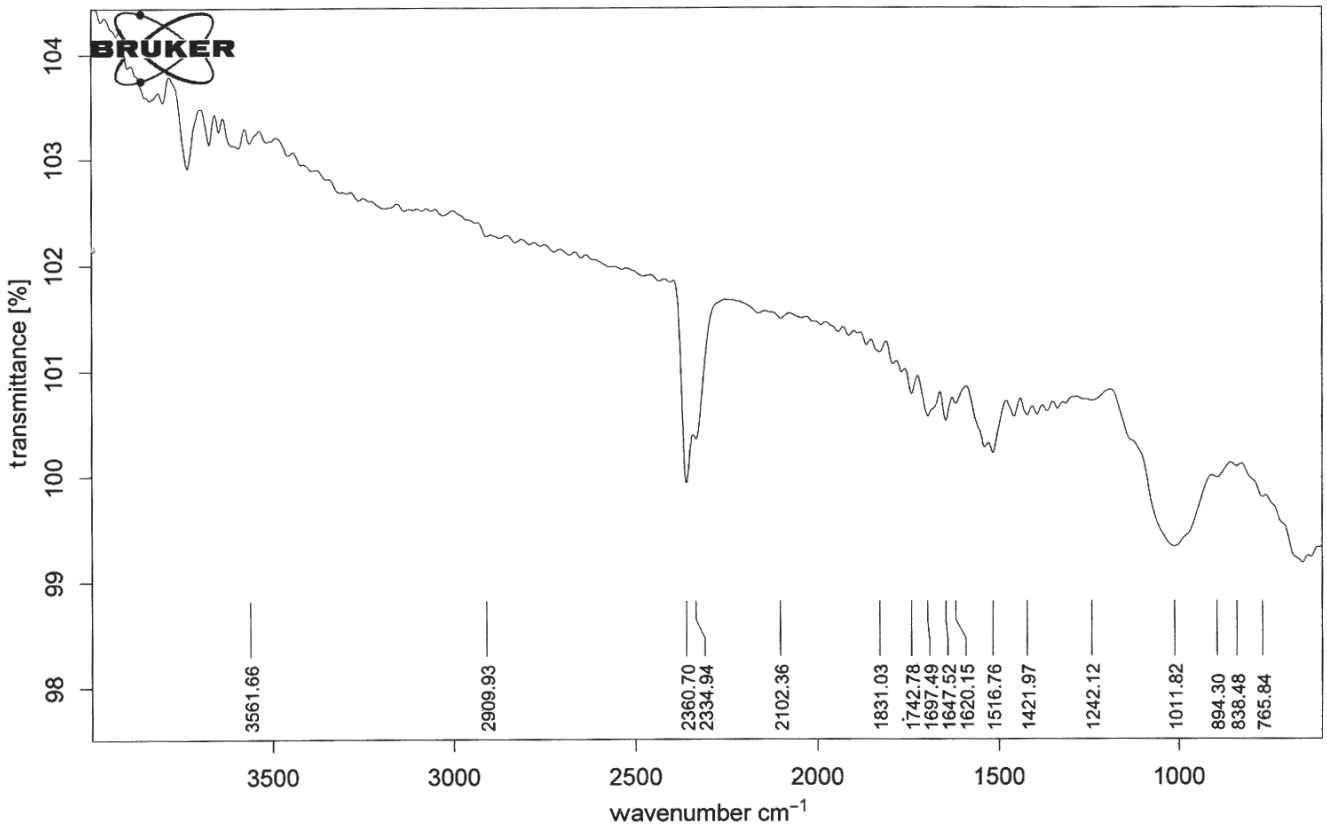

Fig. 4. Infrared spectra of Kheri gum

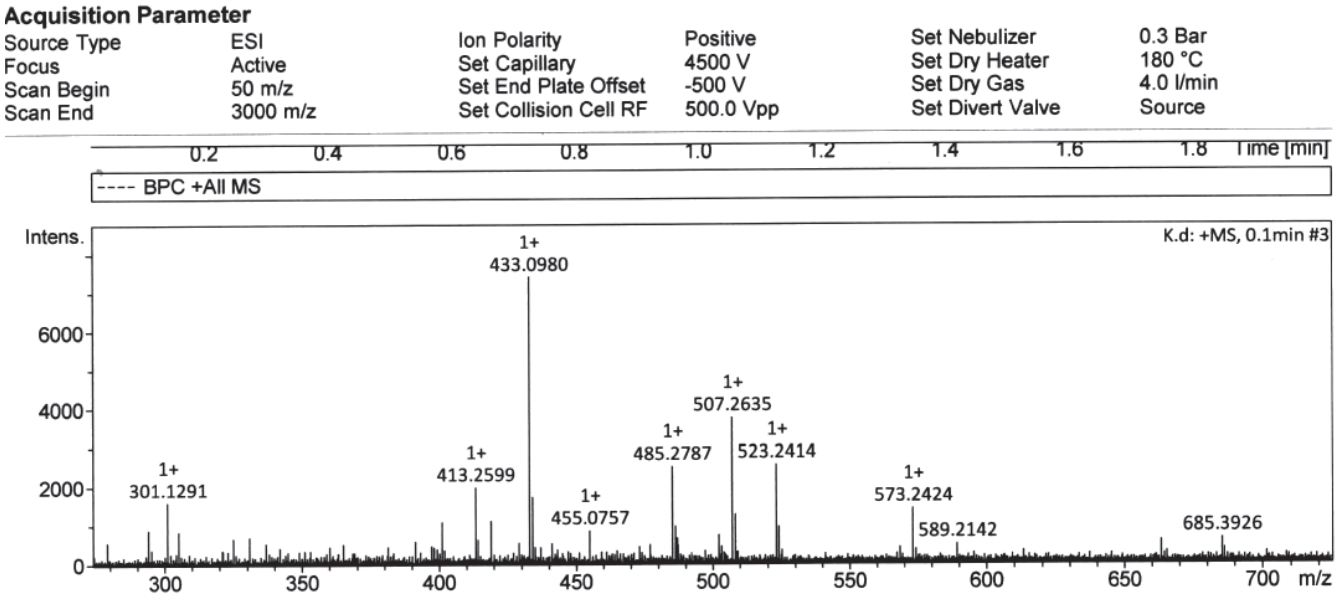

Fig. 5. Mass spectra of Kheri gum

relative to TMS. As shown in spectra (Fig. 6) shift value 5.417 PPM predicts the presence of tetrahydropyran hydrogen (1-alpha–O– from methane, 1-beta–O–C from methane), shift value 4.918 PPM shows the presence of tetrahydropyran hydrogen (1-alpha–O–C– from methane, 1-beta–C– from methane Tetrahydropyran) and the shift value of 3.39 PPM shows the presence of tetrahydropyran hydrogen (1-alpha–O–C– from methane, 1-beta–O–C– from methane, 1-beta–O– from methane). Crowded signals in the ^{1}H NMR spectra of KG are characteristic of polysaccharides and prove the presence of similar sugar residues.

Initially trail batches of suspensions were also prepared using relatively higher concentrations of NGP. It was observed during the study that suspension possesses higher sediment volume at higher concentrations of the polymer (3–7% w/v). It can be concluded from the high sediment volume that the polymer itself becomes a sediment at higher concentrations and it is an undesirable property for a suspension. Further, polymer concentration was reduced to prepare different batches of suspensions, viz. F1, F2, F3, F4 and F5.

Prepared suspensions were white-brown in color with a characteristic odor. The pH of the formulations was found 6.90 ±0.08 to 6.96 ±0.06. On GLMS scale, average value of taste for the prepared suspensions F1, F2, F3, F4 and F5 was found to be "7", "6", "6", "5" and "5" respectively. For odor determination, the intensity scale was used and the intensity level of all the prepared suspensions was marked as "F".

Particle size analysis was carried out with an optical microscope. The effect of concentration of suspending agent (i.e., KG) on the pH and flow rate of suspension was shown in Table 2. It was analyzed from the result that the flow rate decreases as the concentration of KG increases. This is due to the 3-dimensional polymeric structure of the polymer and their more significant interaction at a higher concentration. A significant effect of the NGP on the redespersion time of suspension was observed due to the change in viscosity of suspension. The rate of settling the suspensions were evaluated for 45 days and the data shown in Table 3.

Results showed that sedimentation volume, particle size and redispersion time of the polymer are directly proportional to KG concentration, while reverse case is observed in the case of flow rate.

These studies used a cheap, biodegradable and effective excipient as a suspending agent in pharmaceutical suspensions. Interaction of the polymer with dispersed phase particles depends upon charge, conformation and size of the suspending agent in continuous phase. The suspending agent forms the bridge between the dispersed phase particles, because of the simultane-

Table 2. Characterization parameters of suspensions

Parameters	Formulations				
	F1	F2	F3	F4	F5
pH	6.90 ±0.08	6.92 ±0.07	6.92 ±0.08	6.93 ±0.06	6.96 ±0.06
Flow rate [mL/s]	4.33 ±0.00	4.32 ±0.01	4.32 ±0.00	4.30 ±0.00	4.27 ±0.00
Particle size [μ]	1.29 ±17.03	1.67 ±19.39	1.33 ±23.26	1.43 ±16.00	1.71 ±18.51
Redispersion time [s]	39 ±3.47	45 ±1.33	46 ±2.67	49 ±2.74	53 ±2.56

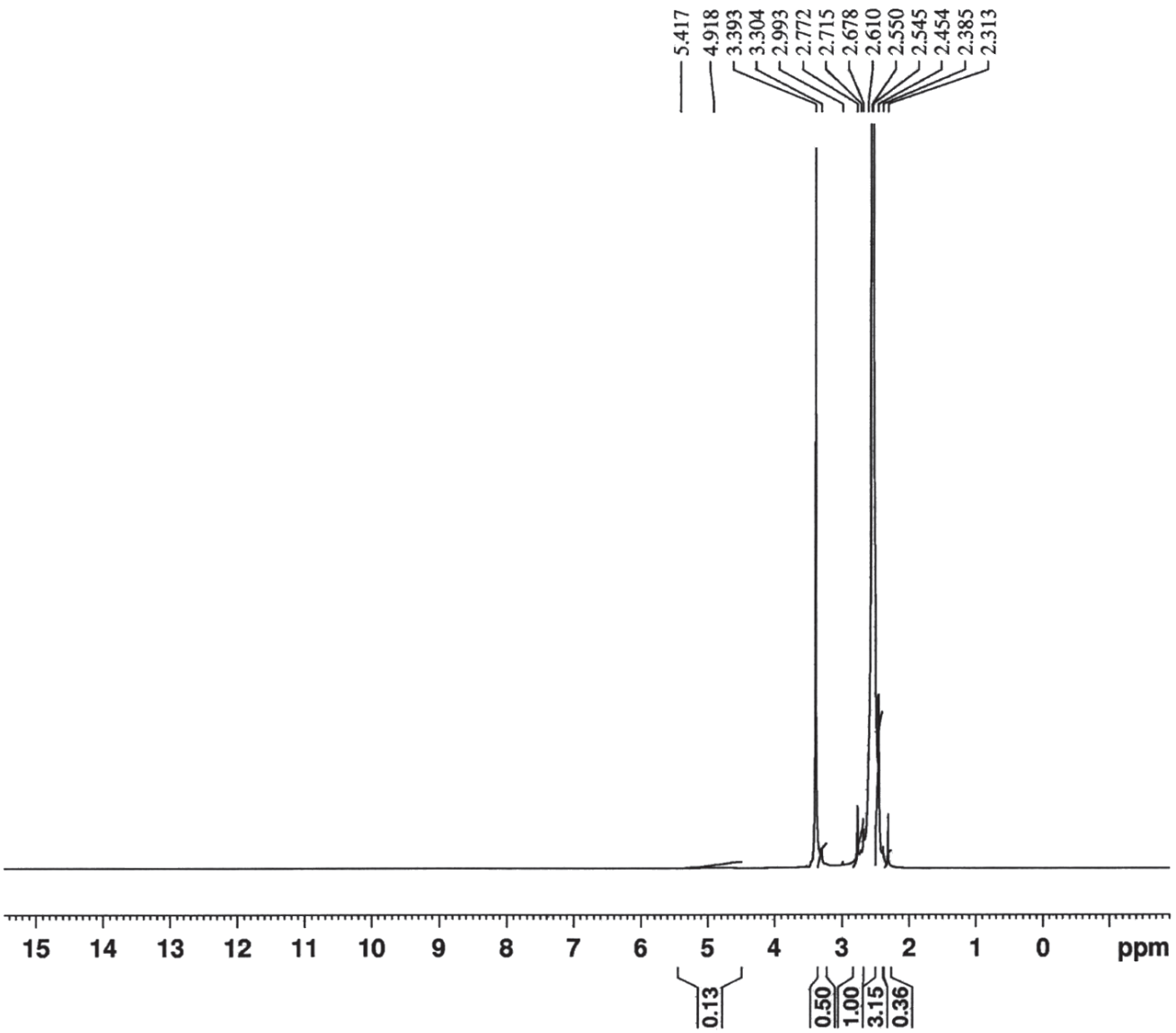

Fig. 6. ^{1}H NMR spectra of Kheri gum polysaccharide

ous adsorption of the suspending agent on the surface of suspended particles. At a low concentration of polysaccharide, less polymer was available to adsorb at the surface of suspended particles hence less number of particle-particle bridges were formed. In this condition the formation of flocculated suspension takes place. Intermediate concentration of KG leads to the formation of more particle-particle bridges and the formation of flocculated suspension. A higher concentration of KG leads to the complete coverage of suspended particles and prevents close particle-particle interaction, leading to the formation of particle-particle bridges. In this condition, deflocculated suspension is formed. After 45 days, no crystal growth was analyzed by particle size analysis. It was observed that there is no significant change in the size of drug particles.

Table 3. Rate of settling of suspensions

Formulation	Sedimentation volume							
	after 1 day	after 2 days	after 3 days	after 4 days	after 5 days	after 15 days	after 21 days	after 45 days
F1	1	1	1	1	1	1	1	0.09
F2	1	1	1	1	1	1	1	0.15
F3	1	1	1	1	1	1	1	0.18
F4	1	1	1	1	1	1	1	0.30
F5	1	1	1	1	1	1	1	0.24

Conclusions

It can be concluded from the findings that:

- KG can be effectively purified using water as a solvent and ethyl alcohol as a precipitating agent.
- KG gum shows the presence of carbohydrate, while fats and volatile oils are absent in polysaccharide.
- Positive value of change in entropy shows a higher number of conformation in dilute solution.
- Dilute solution of KG in water shows rod shaped conformation of polymer.
- IR spectroscopic study shows the presence of free (COO–) and esterified (COO–R) carboxylic acid, ether (C–O stretching), galacturonic acid and mannose in polysaccharide.
- ^{1}H NMR study predicts the presence of tetrahydropyran hydrogen in the molecule.
- Research also provides insights for the use of KG as a suspending agent, because prepared suspensions did not exhibit any significant change in particle size, pH and flow rate during storage.

References

1. Priscilla BSA, Luana CBBC, José AT, Carneiro-da-Cunha MG. Approaches in biotechnological applications of natural polymers. *AIMS Mol Sci.* 2016;3(3):386–425.
2. Malviya R, Sharma PK, Dubey SK. Antioxidant potential and emulsifying properties of Kheri (*Acacia chundra*, Mimosaceae) gum polysaccharide. *Marmara Pharm J.* 2017 [In press].
3. Pant S, Malviya R, Sharma P. Extraction and characterization of *Boswellia serrata* gum as pharmaceutical excipient. *Polim Med.* 2015;45(1):25–30.
4. Malviya R. Extraction characterization and evaluation of selected muclilage as pharmaceutical excipient. *Polim Med.* 2011;41(3):39–44.
5. Indian Pharmacopoeia. 7th ed. New Delhi, India: Government of India, Controller of Publications; 2014:vol. 2.
6. AOAC, 2000. Official methods of analysis. Washington, USA: Association of official analytical chemist.
7. Eddy NO, Udofia I, Uzairu A, Odiongenyi AO, Obadimu C. Physicochemical, spectroscopic and rheological studies on *Eucalyptus citriodora* (EC) gum. *J Polym Biopolym Phys Chem.* 2014;2(1):12–24.
8. Vahid S, Hossein J, Mohammad SY. A comparison of various models for obtaining the intrinsic viscosity of salep gum and sweeteners mixture in dilute solutions. *Int Food Res J.* 2011;18(4):1457–1462.
9. Faria S, de Oliveira Petkowicz CL, Lemos de Moraisc SA, et al. Characterization of xanthan gum produced from sugar cane broth. *Carbohydr Polym.* 2011;88:469–476.
10. Higiro J, Herald T, Alavi S. Rheological study of xanthan and locust bean gum interaction in dilute solution. *Food Res Int.* 2006;39(2):165–175.
11. Nair SV, Oommen Z, Thomas S. Melt elasticity and flow activation energy of nylon 6/polystyrene blends. *Mater Lett.* 2002;57(2):475–480.
12. Morris ER, Cutler AN, Ross-Murphy SB, Rees DA. Concentration and shear rate dependence of viscosity in random coil polysaccharide solution. *Carbohydr Polym.* 1995;1(1):5–21.
13. Arvidson SA, Rinehart BT, Gadala-Maria F. Concentration regimes of solution of levan polysaccharide from *Bacillus* sp. *Carbohydr Polym.* 2006;65:144–149.
14. Spengler B, Dolce JW, Cotter RJ. Infrared laser desorption mass spectrometry of oligosaccharides: Fragmentation mechanisms and isomer analysis. *J Am Chem Soc.* 1990;62(17):1731–1737.

Wpływ starzenia elektrochemicznego na właściwości wybranych pojemników medycznych

Influence of electrochemical ageing on properties of chosen medical receptacles

Adam Gnatowski[A–F], Mateusz Chyra[B], Paulina Walczak[B]

Instytut Technologii Mechanicznych, Politechnika Częstochowska, Polska

A – koncepcja i projekt badania; B – gromadzenie i/lub zestawianie danych; C – analiza i interpretacja danych;
D – napisanie artykułu; E – krytyczne zrecenzowanie artykułu; F – zatwierdzenie ostatecznej wersji artykułu

Polymers in Medicine, ISSN 0370-0747 (print), ISSN 2451-2699 (online) *Polim Med.* 2017;47(2):77–82

Adres do korespondencji
Adam Gnatowski
E-mail: gnatowski@ipp.pcz.pl

Źródła finansowania
Nie występuje

Konflikt interesów
Nie występuje

Praca wpłynęła do redakcji: 05.06.2017 r.
Po recenzji: 11.01.2018 r.
Zaakceptowano do druku: 17.04.2018 r.

Streszczenie

Wprowadzenie. Obecnie większość opakowań stosowanych w medycynie wytwarza się z tworzyw polimerowych. Spowodowane jest to m.in. niską ceną, niewielką masą, jak i walorami estetycznymi gotowych wyrobów. Istotną kwestią jest zapewnienie długiej żywotności tworzywa w celu ochrony zamkniętych w opakowaniach leków.

Cel pracy. Celem pracy była ocena wpływu starzenia elektrochemicznego na właściwości tworzyw polimerowych stosowanych do produkcji opakowań na leki oraz pojemników do zastosowań medycznych.

Materiał i metody. Przeprowadzono analizę porównawczą próbek wyciętych z opakowań na leki wykonanych z polietylenu oraz pojemników do zastosowań medycznych i probówek Eppendorfa wytworzonych z polipropylenu przed procesem starzenia elektrochemicznego oraz po nim. Wykonano badania różnicowej kalorymetrii skaningowej (differential scanning calorimetry – DSC) oraz sfotografowano mikrostrukturę tworzyw w powiększeniu ×400.

Wyniki. Dla próbek, które poddano starzeniu, odnotowano odmienne wartości stopnia krystaliczności w porównaniu z próbkami niestarzonymi. Zarejestrowano również zmiany w wartościach temperatur przemian fizycznych. W próbkach starzonych zauważono także rozdrobnienie struktury krystalicznej.

Wnioski. Tworzywa polimerowe stosowane do produkcji pojemników medycznych poddane procesowi starzenia elektrochemicznego zmieniają swoje właściwości.

Słowa kluczowe: polietylen, polipropylen, właściwości termiczne, struktura

DOI
10.17219/pim/90021

Abstract

Background. Presently, most of receptacles used in medicine are made of polymeric materials. This is due to, e.g., low price, low weight, and aesthetic values of these materials. The important issue is to ensure long life of polymer in order to protect the medicines closed in the boxes. However, all materials during exploitation are exposed to many factors, which can cause degradation of polymer materials. Degradation processes lead to deterioration of thermomechanical properties of polymers.

Objectives. The aim of this syudy was to examine the influence of electrochemical ageing on properties of polymeric materials used in production of receptacles for drugs and boxes for medical use.

Material and methods. We conducted comparative analysis of samples before and after electrochemical ageing, cut out of receptacles for drugs made from polyethylene, as well as from boxes for medical use and Eppendorf tube made from polypropylene. Investigating methods included differential scanning calorimetry (DSC) and imaging of microstructure ×400 magnification.

Results. We noticed different value of the degree of crystallinity for the aged samples in comparison to not aged samples. The change in value of temperature of physical transformation was also detected. In the aged samples defragmentation of crystal structure was observed.

Conclusions. Electrochemical ageing results in changes of properties of polymeric materials used in production of medical receptacles.

Key words: thermal properties, polypropylene, polyethylene, structure

Wprowadzenie

Materiały polimerowe znajdują coraz szersze zastosowanie w przemyśle. Produkowane są z nich zarówno elementy konstrukcyjne, takie jak: koła zębate, łożyska itp., jak i przedmioty codziennego użytku. Tworzywa polimerowe w coraz szerszym stopniu wykorzystywane są również w medycynie. Wytwarza się z nich m.in. strzykawki, soczewki oraz wszelkiego rodzaju pojemniki czy opakowania. Używanie tego typu materiału jest spowodowane m.in. ich niską ceną, niewielką masą, jak i walorami estetycznymi gotowych wyrobów.[1–4] Istotną kwestią jest zapewnienie dużej żywotności tworzywa w celu ochrony zamkniętych w opakowaniach leków. W czasie eksploatacji tworzywo polimerowe narażone jest jednak na wiele czynników mogących powodować jego starzenie. Pojęcie starzenia używane jest do określenia zmian właściwości fizycznych polimerów spowodowanych reakcjami chemicznymi lub fotochemicznymi, w wyniku których dochodzi do rozerwania łańcucha lub sieciowania makrocząsteczek. Do czynników wywołujących powyższe procesy zaliczyć można m.in.: temperaturę, czas obciążenia, rodzaj odkształcenia, działanie prądu w środowisku elektrolitu, promieniowanie UV oraz warunki atmosferyczne. Wymienione powyżej czynniki mogą w znacznym stopniu wpływać na własności chemiczne, fizyczne, mechaniczne i estetyczne tworzyw polimerowych. Może to być przyczyną spadku atrakcyjności wizualnej opakowania oraz wpływać na znajdujące się w nim substancje medyczne.[5–10] Z tego względu bardzo ważnym aspektem są laboratoryjne badania starzenia. Pozwalają one określić wpływ czynnika degradacyjnego na właściwości tworzywa oraz określić jego żywotność.[11]

Celem pracy była ocena wpływu starzenia elektrochemicznego na właściwości tworzyw polimerowych stosowanych do produkcji opakowań na leki oraz pojemników do zastosowań medycznych. Wykonano badania różnicowej kalorymetrii skaningowej (differential scanning calorimetry – DSC) oraz sfotografowano mikrostrukturę materiałów w powiększeniu ×400.

Materiał i metody

Próbki badawcze wycięto z gotowych produktów powszechnie używanych do zastosowań medycznych. Opakowanie na leki (ryc. 1A) zostało wytworzone z polietylenu wysokiej gęstości, natomiast pojemnik do zastosowań medycznych (ryc. 1B) oraz probówkę Eppendorfa (ryc. 1C) wykonano z izotaktycznego polipropylenu.

Część próbek poddano procesowi starzenia elektrochemicznego w specjalnej komorze. Następnie wykonano analizę porównawczą próbek przed starzeniem i po nim. Symulację procesu starzenia przeprowadzono w szkla-

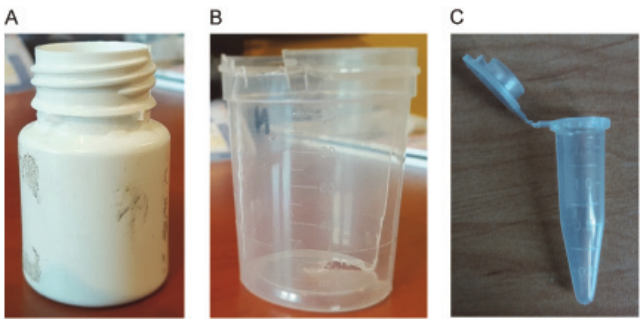

Ryc. 1. A – opakowanie na leki; B – pojemnik do zastosowań medycznych; C – probówka Eppendorfa
Fig. 1. A – receptacle for drugs; B – box for medical use; C – Eppendorf tube

nym naczyniu, w którym znajdował się wodny roztwór chlorku sodu (NaCl) o stężeniu 0,35%. W badaniu użyto elektrod grafitowych. Próbki zanurzono w roztworze na okres 4 tygodni. Podczas badania zastosowano stałą wartość natężenia prądu równą 0,3 A i temperaturę 20°C.

Analizę właściwości termicznych przeprowadzono na urządzeniu DSC 214 Polyma (Netzsch, Exton, USA). Pomiary wykonano, na przemian ogrzewając i chłodząc próbki ze stałą szybkością zmiany temperatury równą 10°C/min. W celu określenia właściwości dla materiału wyjściowego, nieuzależnionych od procesu przetwórstwa i historii termicznej wyrobu, przeprowadzono pomiar z ponownym grzaniem. Program zmian temperatury był następujący:

– grzanie od 20°C do 180°C,
– utrzymanie w stałej temperaturze 180°C przez 2 min,
– chłodzenie od 180°C do –70°C,
– utrzymanie w stałej temperaturze –70°C przez 2 min,
– grzanie od –70°C do 180°C.

Następnie z użyciem oprogramowania Netzsch Proteus (Netzsch, Exton, USA) wyznaczono wartości temperatur przemian fizycznych oraz obliczono wartości stopnia krystaliczności badanych próbek, wyznaczając pole powierzchni pomiędzy krzywą termograficzną a linią podstawy w zakresie występowania refleksu endotermicznego.

Próbki do przeprowadzenia badań strukturalnych wycinano z użyciem mikrotomu rotacyjnego HM 325 firmy Thermo Electron Corporation (USA) przy prędkości cięcia równej 24 µm/s. Grubość próbek z polietylenu wynosiła 12 µm, a ich powierzchnia zawierała się w przedziale 2–4 mm^2. Morfologię polimerów obserwowano pod mikroskopem Nikon Eclipse 2000 (Nikon, Tokio, Japonia) w powiększeniu ×400.

Wyniki

Na ryc. 2–10 oraz w tabelach 1 i 3 przedstawiono wyniki badań DSC dla próbek przed procesem starzenia elektrochemicznego i po nim.

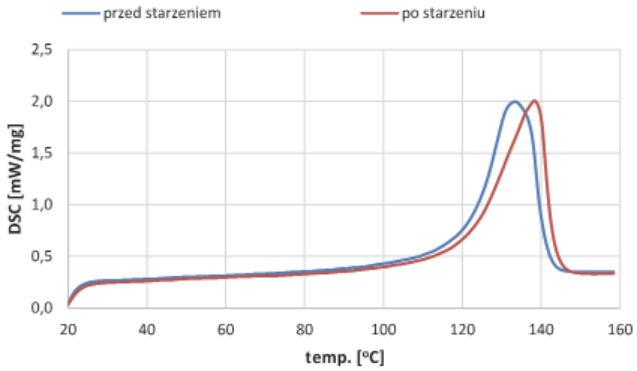

Ryc. 2. Termogramy dla I grzania próbek wyciętych z opakowania na leki przed starzeniem i po nim
Fig. 2. Thermograms for the 1st heating of samples cut from box for drugs before and after ageing

Stopień krystaliczności próbek wyznaczono podczas chłodzenia. Na podstawie badań metodą DSC stwierdzono, że starzenie elektrochemiczne ma wpływ na właściwości próbek. Dla próbek wykonanych z polietylenu na skutek starzenia odnotowano rozszerzenie zakresu temperatury topnienia zarówno w przypadku pierwszego, jak i drugiego grzania. Zakres temperatury krystalizacji uległ natomiast zawężeniu. Podczas

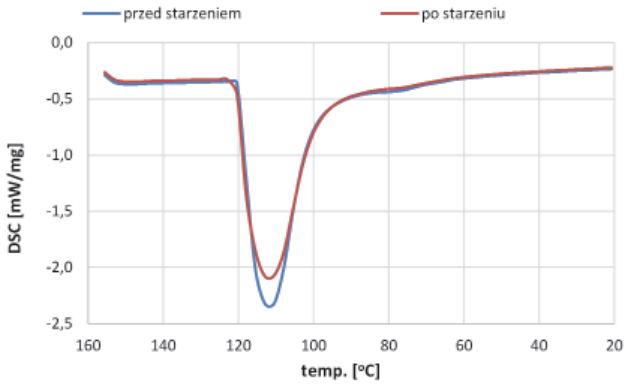

Ryc. 3. Termogramy dla chłodzenia próbek wyciętych z opakowania na leki przed starzeniem i po nim
Fig. 3. Thermograms for cooling of samples cut from box for drugs before and after ageing

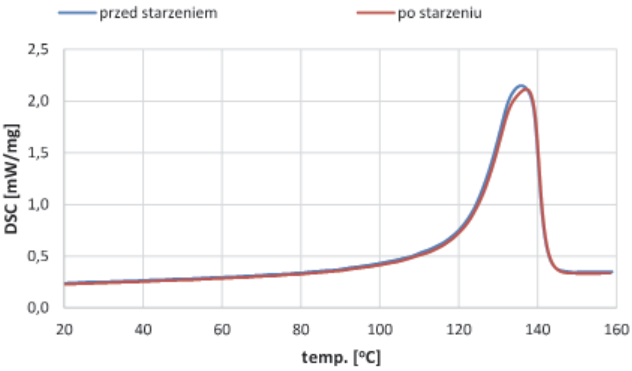

Ryc. 4. Termogramy dla II grzania próbek wyciętych z opakowania na leki przed starzeniem i po nim
Fig. 4. Thermograms for the 2nd heating of samples cut from box for drugs before and after ageing

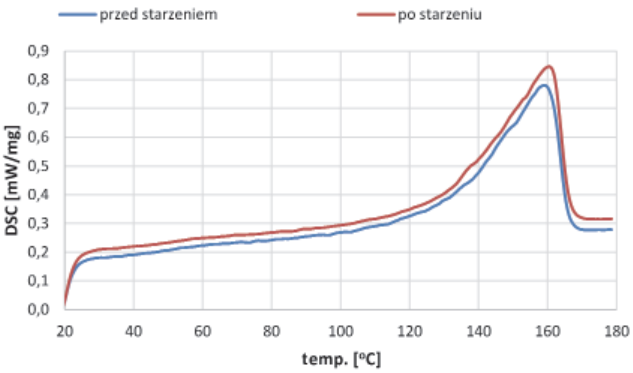

Ryc. 5. Termogramy dla I grzania próbek wyciętych z pojemnika do zastosowań medycznych przed starzeniem i po nim
Fig. 5. Thermograms for the 1st heating of samples cut from box for medical use before and after ageing

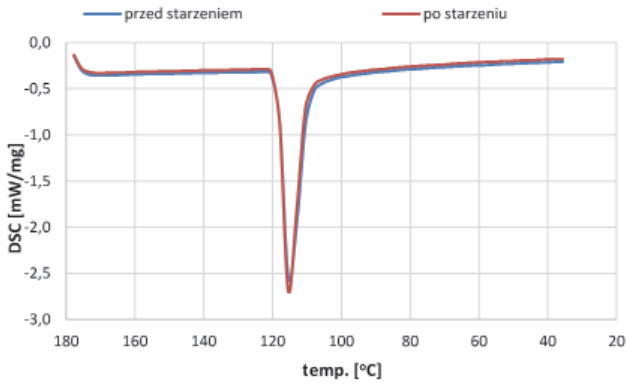

Ryc. 6. Termogramy dla chłodzenia próbek wyciętych z pojemnika do zastosowań medycznych przed starzeniem i po nim
Fig. 6. Thermograms for cooling of samples cut from box for medical use before and after ageing

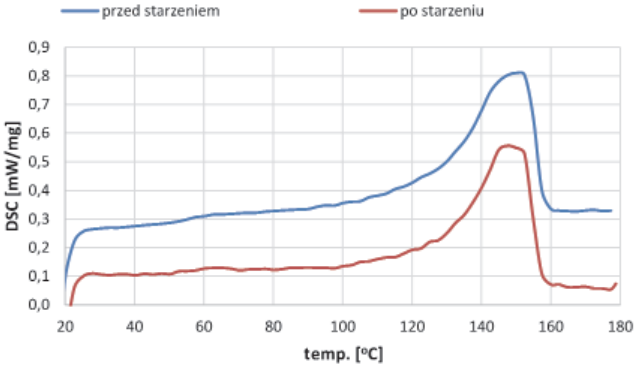

Ryc. 8. Termogramy dla I grzania próbek wyciętych z probówki Eppendorfa przed starzeniem i po nim
Fig. 8. Thermograms for the 1st heating of samples cut from Eppendorf tube before and after ageing

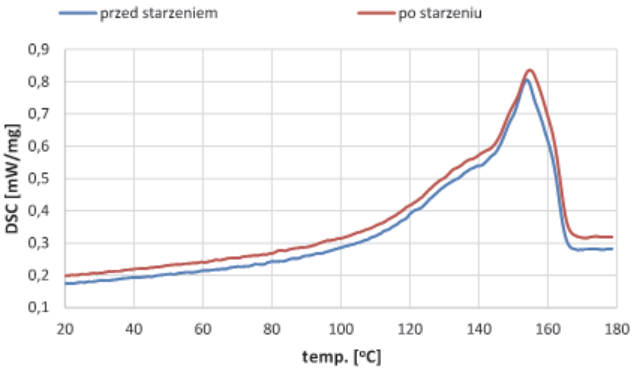

Ryc. 7. Termogramy dla II grzania próbek wyciętych z pojemnika do zastosowań medycznych przed starzeniem i po nim
Fig. 7. Thermograms for the 2nd heating of samples cut from box for medical use before and after ageing

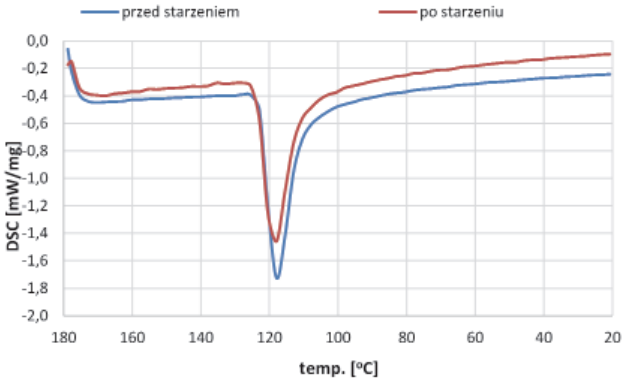

Ryc. 9. Termogramy dla chłodzenia próbek wyciętych z probówki Eppendorfa przed starzeniem i po nim
Fig. 9. Thermograms for cooling of samples cut from Eppendorf tube before and after ageing

Tabela 1. Wyniki analizy różnicowej kalorymetrii skaningowej dla próbek wyciętych z opakowania na leki
Table 1. Results of differential scanning calorimetry (DSC) analysis for the samples cut from the box for drugs

Właściwości materiału polimerowego	Próbki przed starzeniem	Próbki poddane starzeniu
Zakres temperatury topnienia	120,7°C–141,2°C	118,6°C–143,4°C
Zakres temperatury krystalizacji	119,3°C–99,3°C	120,6°C–98,6°C
Zakres temperatury II topnienia	120,6°C–141,1°C	120,4°C–142,3°C
Temperatura, w której topnienie przebiega najszybciej	133,4°C	138,5°C
Temperatura, w której II topnienie przebiega najszybciej	135,9°C	137,3°C
Temperatura, w której krystalizacja przebiega najszybciej	111,8°C	112,1°C
Stopień krystaliczności	60,78%	58,29%

Tabela 2. Wyniki analizy różnicowej kalorymetrii skaningowej dla próbek wyciętych z pojemnika do zastosowań medycznych
Table 2. Results of różnicowej kalorymetrii skaningowej differential scanning calorimetry (DSC) analysis for the samples cut from the box for medical use

Właściwości materiału polimerowego	Próbki przed starzeniem	Próbki poddane starzeniu
Zakres temperatury topnienia	129,1°C–166,1°C	127,8°C–166,1°C
Zakres temperatury krystalizacji	118,4°C–109,5°C	118,4°C–110,4°C
Zakres temperatury II topnienia	134,4°C–165,5°C	137,9°C–165,4°C
Temperatura, w której topnienie przebiega najszybciej	160,3°C	159,2°C
Temperatura, w której II topnienie przebiega najszybciej	154,5°C	154,1°C
Temperatura, w której krystalizacja przebiega najszybciej	115°C	115,1°C
Stopień krystaliczności	34,90%	34,56%

Tabela 3. Wyniki analizy różnicowej kalorymetrii skaningowej dla próbek wyciętych z probówki Eppendorfa
Table 3. Results of differential scanning calorimetry analysis for the samples cut from Eppendorf tube

Właściwości materiału polimerowego	Próbki przed starzeniem	Próbki poddane starzeniu
Zakres temperatury topnienia	124,6°C–157,6°C	126,4°C–156,8°C
Zakres temperatury krystalizacji	122,6°C–110,5°C	123,7°C–110,5°C
Zakres temperatury II topnienia	136,7°C–157°C	136,6°C–157,1°C
Temperatura, w której topnienie przebiega najszybciej	152°C	151,3°C
Temperatura, w której II topnienie przebiega najszybciej	151,9°C	152,3°C
Temperatura, w której krystalizacja przebiega najszybciej	118°C	118,6°C
Stopień krystaliczności	34,69%	30,5%

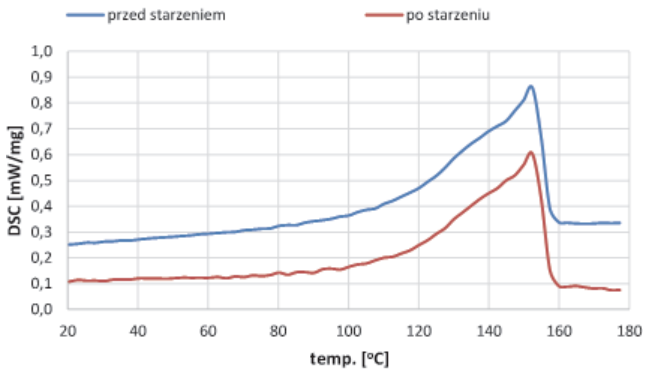

Ryc. 10. Termogramy dla II grzania próbek wyciętych z probówki Eppendorfa przed starzeniem i po nim
Fig. 10. Thermograms for 2nd heating of samples cut from Eppendorf tube before and after ageing

pierwszego grzania zarejestrowano wzrost temperatury o 5°C, w której topnienie fazy krystalicznej przebiega najszybciej. Podczas drugiego grzania wartość temperatury topnienia wzrosła o 2°C. Temperatura, w której krystalizacja tworzywa jest najszybsza, nie uległa istotnej zmianie. W próbkach poddanych procesowi starzenia zarejestrowano o 2% mniejszą wartość stopnia krystaliczności w porównaniu z próbkami niestarzonymi.

W tabeli 2 zestawiono wyniki badań DSC dla próbek wyciętych z pojemników do zastosowań medycznych. Próbki wykonane z polipropylenu charakteryzowały się większą odpornością na starzenie elektrochemiczne niż próbki polietylenowe. W przypadku pierwszego grzania na skutek starzenia odnotowano niewielkie rozszerzenie zakresu temperatury topnienia. W przypadku drugiego grzania zakres ten uległ natomiast nieznacznemu zawężeniu. Podczas chłodzenia nie odnotowano żadnych zmian zakresu temperatury krystalizacji. Nieznaczne różnice zarejestrowano dla wartości temperatury, przy której topnienie fazy krystalicznej przebiega najszybciej w przypadku pierwszego i drugiego grzania. Dla próbek poddanych procesowi starzenia nie odnotowano również znaczącej różnicy temperatury, przy której krystalizacja przebiega najszybciej. Stopień krystaliczności nieznacznie się zmniejszył.

Na ryc. 11 przedstawiono zdjęcia mikrostruktury tworzyw przed procesem starzenia elektrochemicznego i po nim w powiększeniu ×400.

Podczas badań mikroskopowych zarejestrowano zmiany struktury fazowej polimerów. Nastąpił rozrost obszarów amorficznych kosztem gęstości upakowania makrocząsteczek. Oznacza to, że zmniejszyła się liczba ośrodków nukleacji i dzięki temu poszczególne sferolity stały się większe i bardziej widoczne. Uległy zmianom oddziaływania międzycząsteczkowe w łańcuchach, co ograniczyło ruchliwość makrocząsteczek i zwiększyło odległość między skupiskami krystalitów, zmieniając udział poszczególnych faz.

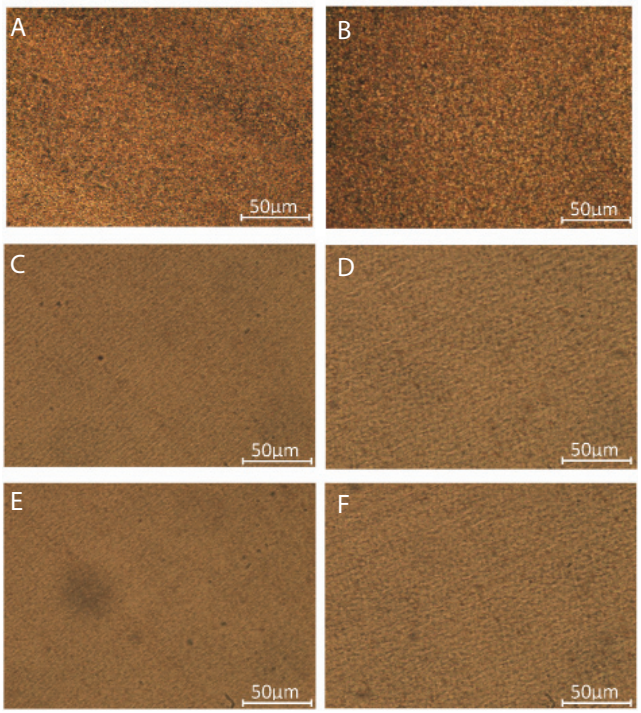

Ryc. 11. Struktura próbek: A – PE przed starzeniem; B – PE po starzeniu; C – PP przed starzeniem (pojemnik); D – PP po starzeniu (pojemnik); E – PP przed starzeniem (probówka Eppendorfa); F – PP po starzeniu (probówka Eppendorfa); PE – polietylen; Pp – polipropylen
Fig. 11. Structure of samples: A – PE before ageing; B – PE after ageing; C – PP before ageing (box); D – PP after ageing (box); E – PP before ageing (Eppendorf tube); F – PP after ageing (Eppendorf tube); PE – polyethylene; PP – polypropylene

Omówienie i wnioski

Na podstawie przeprowadzonych badań można stwierdzić, że starzenie elektrochemiczne ma niewielki wpływ na badane tworzywa polimerowe. Opierając się na rezultatach zastosowania metody DSC, zarejestrowano zmianę właściwości termicznych próbek poddanych procesowi starzenia. Największą zmianę odnotowano w przypadku temperatury topnienia i maksymalnego refleksu dla próbki z polietylenu – przesunięcie w zakres wyższych temperatur. Najmniejsza zmiana nastąpiła dla próbki z polipropylenu w zakresie temperatury krystalizacji oraz temperatury, w której krystalizacja przebiega najszybciej – niewielkie przesunięcie w stronę wyższej temperatury. Zaobserwowano również zmiany w mikrostrukturze tworzyw podczas badania pod mikroskopem optycznym. Zarówno w próbce z polietylenu, jak i polipropylenu zmieniła się krystaliczność związana ze spadkiem ruchliwości makrocząsteczek. Zmniejszenie się oddziaływań międzycząsteczkowych może powodować zaburzenia w sekwencji łańcuchów, co prowadzi do spadku stopnia krystaliczności. Ponadto oddziaływania międzycząsteczkowe mają wpływ na udział poszczególnych faz strukturalnych oraz na rozmiar sferolitów i odległości między nimi.

Wzrost udziału fazy amorficznej kosztem fazy krystalicznej powoduje zmniejszenie gęstości tworzywa. Pogorszeniu ulegają właściwości mechaniczne i plastyczne, a co za tym idzie – właściwości użytkowe materiałów. Może nastąpić spadek ich twardości, odporności na ścieranie czy wytrzymałości na rozciąganie.

Piśmiennictwo

1. Hyla I. *Tworzywa sztuczne. Własności, przetwórstwo, zastosowanie*. Gliwice, Poland: Wydawnictwo Politechniki Śląskiej; 2000.
2. Neffe AT, Grijpma DW, Lendlein A. Advanced functional polymers for medicine. *Macromol Biosci*. 2016;16(12):1743–1744.
3. Klepka T, Zgierski P. Charakterystyka metod wtryskiwania do zastosowań medycznych. *Post Nauk Tech*. 2011;8:192–200.
4. Fizia-Orlicz A, Misiuk-Hojło M. Soczewki wewnątrzgałkowe w chirurgii zaćmy: Wykorzystanie polimerów. *Polim Med*. 2015;2:95–102.
5. Michalska-Pożoga I. Proces starzenia a właściwości przetwórcze PE-LD po wielokrotnym wytłaczaniu. *Przetwórstwo Tworzyw*. 2012;5:541–545.
6. White JW. Polymer ageing: Physics, chemistry or engineering? Time to Reflect. *C R Chim*. 2006;9:1396–1408.
7. Gnatowski A, Chyra M. Effect of electrochemical ageing on the properties of polyamide composites with glass fiber and quartz sand. *Przemysł Chemiczny*. 2015;1(94):103–106.
8. Grabowska B. Biodegradacja tworzyw polimerowych. *Arch Foun Engineer*. 2010;10(2):57–60.
9. Sobków D, Czaja K. Wpływ warunków przyspieszonego starzenia na proces degradacji poliolefin. *Polimery*. 2003;9:627–632.
10. Tochacek J, Vratnickova Z. Polymer life-time prediction: The role of temperature in UV-accelerated ageing of polypropylene and its copolymers. *Polym Test*. 2014;36:82–87.
11. Jachowicz T, Sikora R. Metody prognozowania zmian właściwości wytworów z tworzyw polimerowych. *Polimery*. 2006;3:177–185.

Improving the solubility of nevirapine using A hydrotropy and mixed hydrotropy based solid dispersion approach

Jyotsana R. Madan[1,A–F], Virendra J. Kamate[1,A–F], Kamal Dua[2,3,4,A,C–F], Rajendra Awasthi[5,A,C–F]

[1] Department of Pharmaceutics, Sinhgad Technical Education Society's, Smt. Kashibai Navale College of Pharmacy, Pune, Maharashtra, India
[2] Discipline of Pharmacy, Graduate School of Health, University of Technology Sydney, Sydney, Australia
[3] School of Pharmacy and Biomedical Sciences, The University of Newcastle, Newcastle, Australia
[4] School of Pharmaceutical Sciences, Shoolini University, Solan, India
[5] NKBR College of Pharmacy & Research Centre, Meerut, India

A – research concept and design; B – collection and/or assembly of data; C – data analysis and interpretation;
D – writing the article; E – critical revision of the article; F – final approval of the article

Polymers in Medicine, ISSN 0370-0747 (print), ISSN 2451-2699 (online) *Polim Med.* 2017;47(2):83–90

Address for correspondence
Jyotsana R. Madan
E-mail: jyotsna.madan@sinhgad.edu

Funding sources
none declared

Conflict of interest
none declared

Received on June 15, 2017
Reviewed on July 4, 2017
Accepted on September 19, 2017

Abstract

Background. Nevirapine, an antiviral drug, is a potent reverse transcriptase inhibitor (NNRTI). It is used in combination with nucleoside analogues for treatment of HIV type-1 (HIV-1) infection and AIDS. Nevirapine is a BCS class II drug which shows dissolution rate limited absorption.

Objectives. The aim of the present research was to provide a fast dissolving solid dispersion of nevirapine.

Material and methods. The solubility of nevirapine was initially determined individually in four hydrotropic agents – namely urea, lactose, citric acid and mannitol – at a concentration of 10, 20, 30 and 40% w/v solutions using purified water as a solvent. The highest solubility was obtained in the 40% citric acid solution. Then different combinations of 2 and 3 hydrotropic agents in different ratios were used to determine solubility, so that the total concentration of hydrotropic agents was always 40%.

Results. The highest solubility was obtained in a solution of lactose and citric acid at the optimum ratio of 15:25. This optimized combination was utilized in preparing solid dispersions by a common solvent technique using distilled water as a solvent. The solid dispersions were evaluated for XRD, DSC and FTIR to show no drug-hydrotrope interaction.

Conclusions. It was concluded that the concept of mixed hydrotropic solid dispersion is a safe, novel and cost-effective technique for enhancing the bioavailability of poorly water-soluble drugs by dissolving the drug in a nonionized form. The enhancement in solubility of nevirapine using hydrotropy is a clear indication of its potential to be used in the future for other poorly water-soluble drugs in which low bioavailability is a major concern.

Key words: nevirapine, solid dispersion, mixed hydrotropy

DOI
10.17219/pim/77093

One of the important phenomena in pharmaceutical formulation is "solubility", which plays very effective and significant role in the formulation of various dosage forms.[1,2] The solubility of a compound in a particular solvent is defined as the concentration of a solute in a saturated solution at a certain temperature.[3,4] The solubility of a drug molecule may be a critical factor determining its usefulness since the solubility dictates the amount of compound that will dissolve and therefore the amount available for absorption. If a compound has low water solubility, it may be subject to dissolution rate limited absorption within the gastrointestinal residence time.[5,6] The term "hydrotrope" was introduced by Neuberg in 1916. A hydrotropic agent is a compound that solubilizes hydrophobic compounds in aqueous solutions. Hydrotropy is a molecular phenomenon whereby the adding of a large amount of a second solute (hydrotrope) results to an increase in the aqueous solubility of poorly soluble solutes.[7,8] Hydrotropes possess a hydrophobic as well as a hydrophilic group. The hydrophobic part is too small to cause spontaneous self-aggregation. The efficiency of a hydrotropic agent depends on the balance between hydrophobic and hydrophilic parts of the hydrotrope. Finding the right hydrotropic agent for a certain poorly soluble drug necessitates a screening of numerous hydrotropic agents based on the balance between hydrophobic and hydrophilic parts. The presence of a large hydrophobic part leads to better hydrotropic efficiency.[9] The enhancement of aqueous solubility by a hydrotropic agent is based on 1) molecular self-association of the hydrotropic agent and 2) the association of hydrotrope molecules with the solute.[10] Mixed hydrotropic solubilization has great potential to improve the solubility of poorly water soluble molecules.[11–13]

Nevirapine (NVP), an antiviral drug, is a potent reverse transcriptase inhibitor (NNRTI). It is used in combination with nucleoside analogues for the treatment of HIV type-1 (HIV-1) infection and AIDS. It is a BCS class II drug with high permeability and low solubility (aqueous solubility 0.09941 mg/mL).[14,15] The solubility of NVP was increased by using a mixed hydrotropic solid dispersion technique. Here, two or more hydrotropic blends were used, which gives a synergistic solubility enhancement effect on poorly water soluble drugs. The individual concentrations of hydrotropic agents are reduced, thus minimizing the probability of their toxicity.[16,17]

The aim of this research was to enhance the solubility of NVP in water by making use of hydrotropes and their combination blends to prepare its solid dispersion.

Material and methods

Material

The NVP was gifted by Wockhardt Ltd., Aurangabad, India. Urea, sodium benzoate, citric acid, lactose and mannitol were purchased from Loba Chem Pvt. Ltd., Mumbai, India. All reagents were of analytical grade and used as received.

Methods

Determination of solubility

The saturation solubility of NVP was determined with distilled water. An excess amount of NVP was added to each medium and kept in an incubator shaker at 200 rpm for 24 h. The temperature was maintained at 37°C. After 24 h the mixture was centrifuged at 2000 rpm for 10 min. The supernatants were diluted using distilled water. The absorbance of samples was measured at 282 nm for distilled water using a UV spectrophotometer (JASCO V-630, Tsukuba, Japan).[18,19]

NVP-hydrotropic agent interference study

UV spectrophotometric study

Interference of the hydrotropic agents was estimated using the UV spectrophotometric method. Briefly, the absorbance of NVP standard solutions were determined in distilled water alone and in the presence of the hydrotropic blend, respectively (Table 1). The absorbance was recorded against respective blank medium at appropriate wavelengths. A UV-visible spectrophotometer (JASCO V-630) with 1 cm matched silica cells was employed for spectrophotometric estimations.[20]

Fourier-transform infrared spectroscopy (FTIR)

The FTIR spectral data of NVP, physical mixtures of NVP and individual hydrotropes and NVP with two

Table 1. Results of drug-hydrotrope interference study by UV spectrophotometric method

Drug	Solvent system	Drug conc. [µg/mL]	Hydrotrope conc. [µg/mL]	Wavelength [nm]	Absorbance against blank
NVP	dist. water + P	50	1000	282	0.233
NVP	dist. water + Q	50	1000	282	0.256
NVP	dist. water + R	50	1000	282	0.223
NVP	dist. water + S	50	1000	282	0.219
NVP	dist. water	50	1000	282	0.201

P – lactose; Q – urea; R – citric acid; S – mannitol.

hydrotropes were taken for the determination of possible molecular interaction between the drug and excipients by the KBr disc method using an FTIR spectrophotometer (Shimadzu Affinity-1, Kyoto, Japan). The samples were scanned over a range 4000–400 cm^{-1}.[21]

Equilibrium solubility studies in different hydrotropic agents

Initially the equilibrium solubility studies were carried out in different hydrotropic agents. The aqueous hydrotropic solutions of lactose (P), urea (Q), citric acid (R) and mannitol (S) were prepared individually at a concentration of 10, 20, 30 and 40% w/v. Accurately measured 10 mL of a particular blend of hydrotropic agent was taken in a 10 mL vial, and an excess amount of NVP was added and mechanically shaken until a saturated solution was formed. The vial was shaken on a mechanical shaker for 12 h and the solution was allowed to equilibrate for 24 h to achieve equilibrium solubility. The resultant solution was centrifuged at 2000 rpm for 10 min in an ultracentrifuge and further filtered through Whatman grade 41 filters. An aliquot was diluted with distilled water and analyzed using a UV spectrophotometer at 282 nm.[22,23] Enhancement ratios in solubility were calculated by the following formula:

$$\text{enhancement ratio} = \frac{\text{solubility of drug in hydrotropic solution}}{\text{solubity of drug in water}}.$$

Similarly, the equilibrium solubility studies were carried out in different blends of hydrotropic agents. Here, the combinations of 2–3 hydrotropic agents were taken at a 1:1 ratio and dissolved in water to get a clear solution. An excess amount of NVP was added to the hydrotropic solution. The saturated solution was mechanically shaken and aqueous solubility was determined. Further, the ratio of the mixed hydrotropic agent was optimized to achieve the highest aqueous solubility of NVP.

Formulation of hydrotropic solid dispersions of NVP

For the preparation of the hydrotropic solid dispersion (1:4 ratio), accurately weighed 1.5 g lactose and 2.5 g of citric acid were taken in a 100 mL beaker and mixed properly. A sufficient quantity of freshly prepared demineralized water (5 mL) was added to dissolve the hydrotropic mixture. Dissolution of the hydrotropic mixture was facilitated by the agitation of a Teflon coated magnetic rice bead on a high speed magnetic stirrer. After complete dissolution of the hydrotropic mixture, 1 g of NVP was dissolved in the above solution and the temperature was maintained at 57 ±2°C to evaporate the water. As evaporation proceeded, the speed of the rice bead automatically decreased and it stopped stirring when most of the water was evaporated, thus indicating the formation of the solid dispersion (wet). The wet solid dispersion was kept in a hot air dry oven maintained at 50 ±2°C to remove the remaining moisture. After a complete drying, the solid dispersion was crushed using a clean and dry glass mortar and pestle, passed through a #60 sieve and finally stored in an airtight glass bottle.[24–26]

Evaluation of hydrotropic solid dispersion containing NVP

Micromeritic properties of solid dispersions

The prepared hydrotropic solid dispersion was characterized for various micromeritic properties such as bulk density, tapped density, compressibility index, Hausner ratio and angle of repose.[27,28]

For the determination of density, the solid dispersion sample (1 g) was taken into a 10 mL graduated measuring cylinder and the initial volume was noted down. The graduated measuring cylinder was tapped 50 times using USP bulk density apparatus (ETD 1020, Electrolab, Mumbai, India). The bulk density and tapped density were determined using the following formula:

$$\text{bulk density } (g/cm^{-3}) = \frac{\text{weight of the solid dispersion}}{\text{initial volume}},$$

$$\text{tapped density } (g/cm^{-3}) = \frac{\text{weight of the solid dispersion}}{\text{volume after tapping}}.$$

The compressibility index was determined by the following formula:

$$\text{compressibility index} = \frac{\text{tapped density} - \text{bulk density}}{\text{tapped density}} \times 100.$$

The Hausner ratio was determined by the following formula:

$$\text{Hausner's ratio} = \frac{\text{tapped density}}{\text{bulk density}}.$$

For the determination of angle of repose, the solid dispersion was poured through a funnel. The funnel was fixed at a position in such a way that its lower tip was at a height of 2 cm above the surface. The sample was poured till the tip of the particle pile surface touched the funnel. The $\tan^{-1}$ of the ratio of the height of the pile and radius of its base gave the angle of repose. The angle of repose was determined by the following formula:

$$\tan^{-1} = \frac{h}{r}.$$

X-ray powder diffraction analysis

The X-ray diffraction pattern of pure NVP and a physical mixture of the drug and hydrotropic agents (lactose + citric acid) was recorded by X-ray powder diffractometer (Philips 1710). The X-ray diffraction patterns were recorded using Cu-Ka radiation (λ = 1.5405980Å), a current of 30 mA and a voltage of 40 kV. The samples were analyzed, over 10–89 2 theta, range with a scan step size of 0.02 and 0.50 s per step.[29,30]

Differential scanning calorimetry analysis

In order to determine the physical state of the NVP, the differential scanning calorimetry (DSC) thermograms of pure NVP and physical mixture of the drug and hydrotropic agents (lactose + citric acid) was recorded using a differential scanning calorimeter (DSC 4000, PerkinElmer, Waltham, Massachusetts, USA). The instrument was calibrated using indium (156°C), tin (232°C) and zinc (419.5°C) as internal standards. An empty aluminum pan was used as a reference. Each sample was accurately weighed into an aluminum pan and sealed. The probes were heated from 30 to 300°C at a rate of 10 K/min under a nitrogen atmosphere.[31,32]

Results and discussion

Determination of solubility

The solubility of NVP as observed in distilled water was 0.0994 ±0.056 mg/mL. The results indicate poor solubility of NVP in distilled water.

NVP hydrotropic agent interference study

Ultraviolet spectrophotometric study

To examine the interference of a hydrotropic agent, the UV absorbance spectrum of NVP was recorded in distilled water alone and in the presence of the hydrotropic blend solutions. The results indicated no change in the wavelength of maximum absorbance (λ_{max}) of NVP in distilled water. Hence, it was concluded that there was no drug-hydrotrope interference.

Fourier-transform infrared study

Fourier-transform infrared study was employed to examine the possible interactions of NVP and the hydrotropes. The FTIR spectrum of NVP showed characteristic peaks at 3400 cm^{-1} of N–H (secondary amine) stretch, 3190 cm^{-1} of C–H (aromatic) stretch, 3062 cm^{-1} of C–H (aliphatic) stretch, 1647 cm^{-1} of C=O cm^{-1} (ketone) stretch, 1587–1417 cm^{-1} of C=C stretch and 1296 cm^{-1} of C=O (ketone) bending. All peaks are within the reported range, indicating the purity of NVP.[33,34] All the major peaks of NVP are also present in the FTIR spectrum of the hydrotropic physical mixture. Hence, there were no drug-excipient interactions (Fig. 1).

Equilibrium solubility studies in different hydrotropic agents

The equilibrium solubility of NVP in the presence of different hydrotropic agents was investigated as shown in Table 2. All hydrotropes, viz. lactose, urea, citric acid and mannitol, are able to enhance the solubility of NVP. The highest solubility was obtained in the 40% citric acid solution. Then, in order to decrease the concentration of citric acid, different combinations of the above-mentioned four hydrotropic agents in different ratios were tried to determine the enhancement in solubility, so that the total concentration of hydrotropic agents was always 40% w/v. All the hydrotrope blends were also found to increase the solubility of NVP (Table 3). The blend P + R (lactose: citric acid) at a ratio of 5 : 35 gave the highest solubility enhancement, but the concentration of citric acid in this blend is not within the inactive ingredients guidelines (IIG) limit for a single tablet (500 mg/tablet),[17,35] so the ratio of 15 : 25 was chosen, and therefore, this optimized combination of hydrotropes was selected for the preparation of solid dispersion (Table 4).

Micromeritic properties of solid dispersions

The closeness of values of tapping density and bulk density indicates the free-flowing property (Table 5). The difference in bulk density and tapped density was only 0.092, indicating that the change in volume is very small even after 50 tappings, which confirms the small particle size

Table 2. Equilibrium solubility* of NVP in different hydrotropic agents. The data presents mean ± SD, n = 3

Hydrotropic Agents	Concentration (w/v)				Solubility enhancement ratio
	10%	20%	30%	40%	
Lactose (P)	1.07 ±0.121*	1.09 ±0.101	1.09 ±0.111	1.13 ±0.126	11.36 ±1.62
Urea (Q)	1.39 ±0.152	1.80 ±0.094	2.34 ±0.121	2.74 ±0.125	27.16 ±3.54
Citric acid (R)	2.57 ±0.180	3.80 ±0.122	4.70 ±0.054	4.18 ±0.123	42.04 ±1.92
Mannitol (S)	0.94 ±0.051	0.96 ±0.161	0.99 ±0.154	1.01 ±0.122	10.15 ±2.34

* Solubility in mg/mL; P – lactose; Q – urea; R – citric acid; S – mannitol.

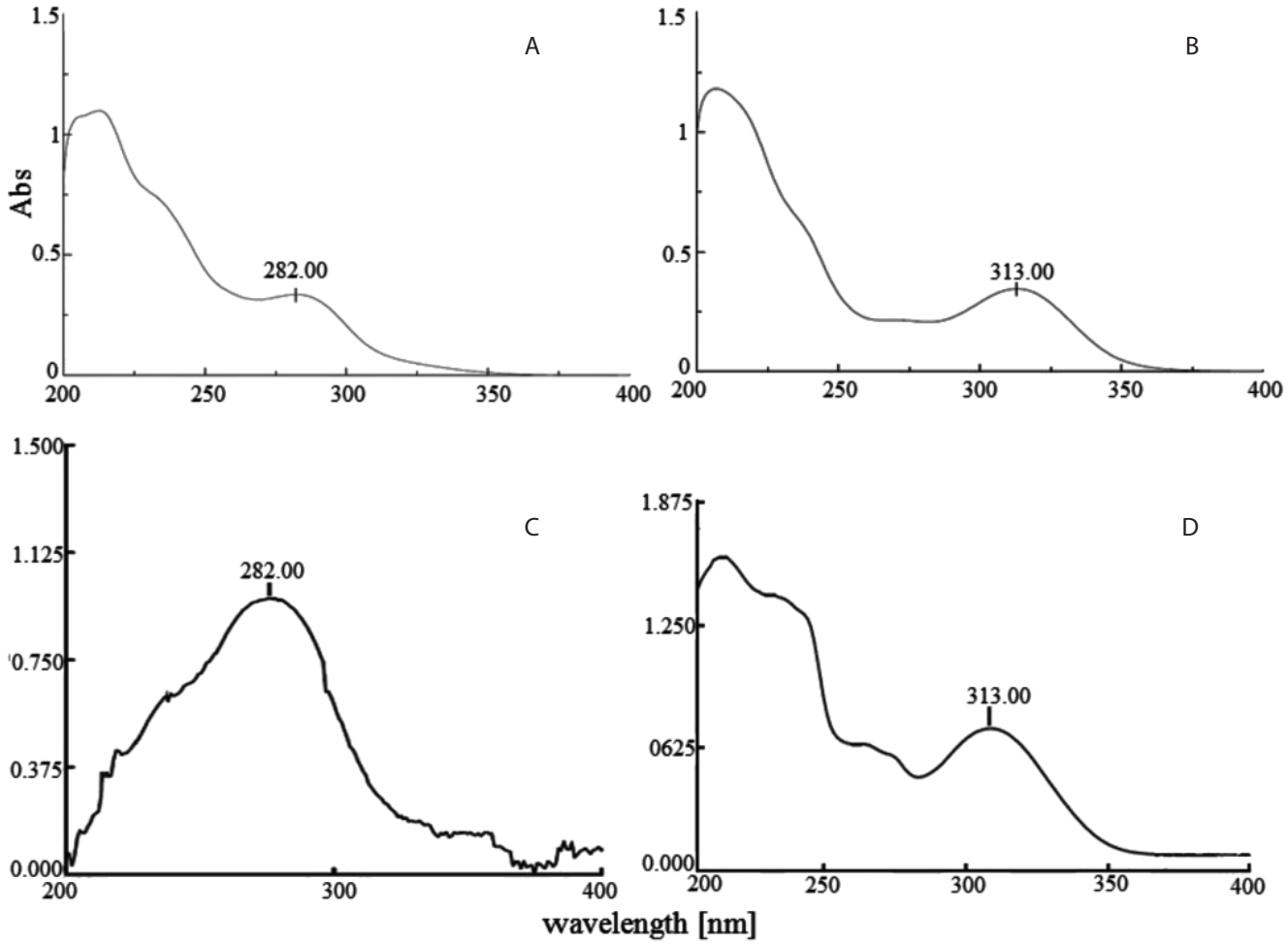

Fig. 1. UV spectra of pure NVP in (A) distilled water, (B) 0.1N HCl, (C) NVP hydrotropic solid dispersion (lactose-citric acid) in distilled water and (D) NVP hydrotropic solid dispersion (lactose-citric acid) in 0.1N HCl

range and reproducibility in drug content.[27,36] It is frequently experienced that particle size and shape influences flowability. The fine particles (< 100 mm) tend to be more cohesive and therefore less free-flowing, whereas larger, denser particles tend to be free-flowing. The rougher and more irregular the surface of the particles, the higher the angle of repose will be.[22] In the present study, the angle of repose was 33°, indicating good flowability of particles. A high compressibility index is indicative of the tendency to form bridges between the particles. The smaller the compressibility index, the better the flow properties will be. For example, a value of 5–15 indicates excellent flow, 12–18 good, 19–21 fair, 22–35 poor, 36–40 very poor and > 40 extremely poor.[22] The results show that the solid dispersion powder had a compressibility index of 11.429, indicating excellent flow property. Hausner ratio is related to inter-particle friction. It is also an indirect measure of bulk density, size and shape, surface area, moisture content and

Table 3. Results of equilibrium solubility of NVP in 1:1 mixed hydrotropic blends. The data presents mean ± SD, n = 3

Combinations	Total conc. [% w/v]	Individual conc. [% w/v]	Solubility [mg/mL]	Solubility enhancement ratio
P + Q	40.00	20.00	2.950 ±0.101	29.67 ±2.51
P + R	40.00	20.00	6.372 ±0.212	64.07 ±1.64
P + S	40.00	20.00	3.083 ±0.052	31.01 ±2.09
Q + R	40.00	20.00	2.640 ±0.184	26.55 ±1.54
Q + S	40.00	20.00	2.907 ±0.152	29.04 ±2.18
R + S	40.00	20.00	2.945 ±0.098	29.62 ±1.72
P + Q + R	40.00	13.33	1.1967 ±0.954	12.03 ±1.08
P + Q + S	40.00	13.33	1.4551 ±0.574	14.63 ±0.81
P + R + S	40.00	13.33	1.4776 ±0.854	14.86 ±1.25
Q + R + S	40.00	13.33	1.9677 ±0.799	19.79 ±2.04

P – lactose; Q – urea; R – citric acid; S – mannitol.

Table 4. Equilibrium solubility of NVP in mixed hydrotropic blends at different ratios. The data presents mean ± SD, n = 3

Combinations	Total conc. [% w/v]	Ratio	Solubility [mg/mL]	Solubility enhancement ratio
P + R	40.00	05 : 35	10.654 ±0.854	107.13 ±7.64
P + R	40.00	10 : 30	10.022 ±0.965	100.81 ±5.34
P + R	40.00	15 : 25	10.174 ±0.745	102.31 ±5.64
P + R	40.00	20 : 20	07.761 ±0.854	78.06 ±8.24
P + R	40.00	25 : 15	05.777 ±0.261	58.04 ±3.51
P + R	40.00	30 : 10	05.258 ±0.350	52.81 ±5.34
P + R	40.00	35 : 05	02.101 ±0.480	21.13 ±3.64

P – lactose; Q – urea; R – citric acid; S – mannitol.

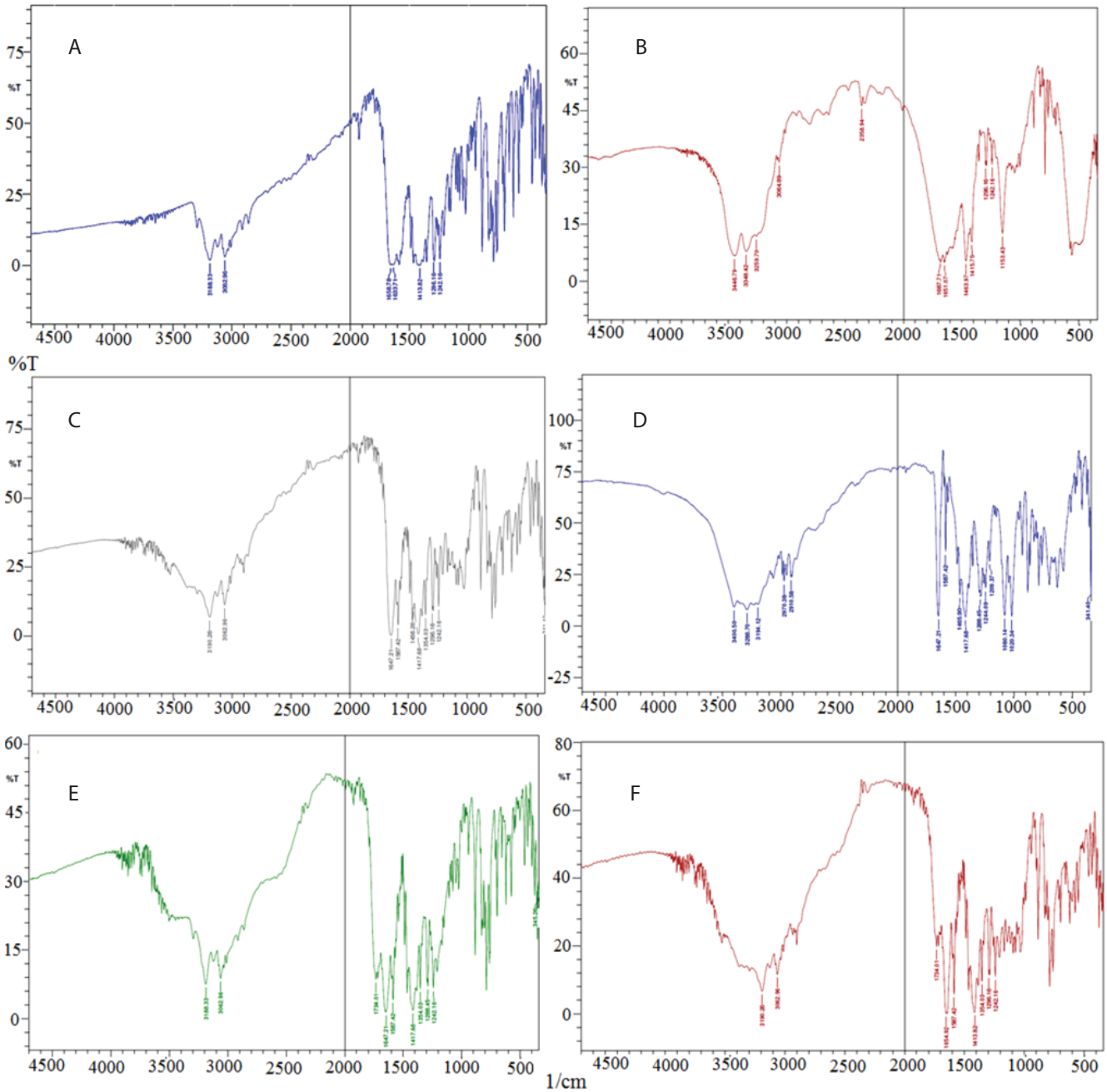

Fig. 2. Fourier transform-infrared spectra of (A) NVP, (B) nevirapine + urea, (C) nevirapine + lactose, (D) nevirapine + mannitol, (E) nevirapine + citric acid and (F) NVP + citric acid + lactose

Table 5. Micromeritic properties of NVP solid dispersions. The data presents mean ± SD, n = 3

Parameter	Result
Bulk density (g/cm^3)	0.714 ±0.01
Tapped density (g/cm^3)	0.806 ±0.03
Compressibility index	11.429 ±2.31
Hausner ratio	1.12 ±0.14
Angle of repose	33 ±1°

cohesiveness of particles. A higher Hausner ratio and more fine particles indicate greater cohesion between particles while a low range indicates good flowability. The desirable value of Hausner ratio is < 1.25 for good flow of materials.[22] In the present study, the Hausner ratio for the solid dispersion powder was found to be 1.12 indicating good flowability of particles. This result was also supported by an angle of repose study. These results indicate that the flow character of the solid dispersion is good and no aid is needed to increase the flow properties.

X-ray diffraction analysis of NVP

It is generally stated that if three consecutive relative intensity percentage values in an XRD pattern decrease, a decrease in crystallinity had occurred in the samples, therefore, these observations can be treated as confirmation of the reduction in crystallinity and thus phase transition.[37] As it is reported that an amorphous system is responsible for the enhancement in dissolution and bioavailability,[38] less intense peaks in the solid dispersion as compared to the NVP pure drug indicate an amorphous nature, explaining the higher solubility of SD as compared to NVP (Fig. 2). These observations were in accordance with the DSC studies (Fig. 3).

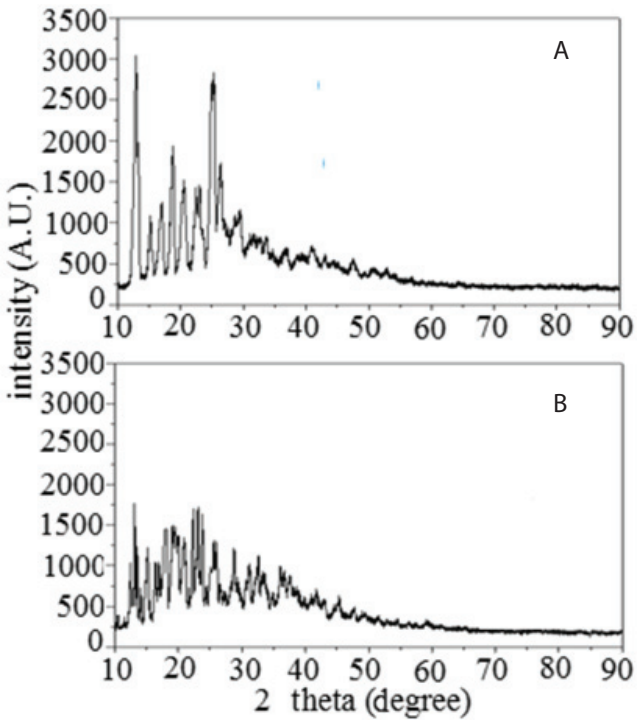

Fig. 3. X-ray powder diffraction spectra of (A) NVP and (B) NVP hydrotropic solid dispersion (lactose-citric acid)

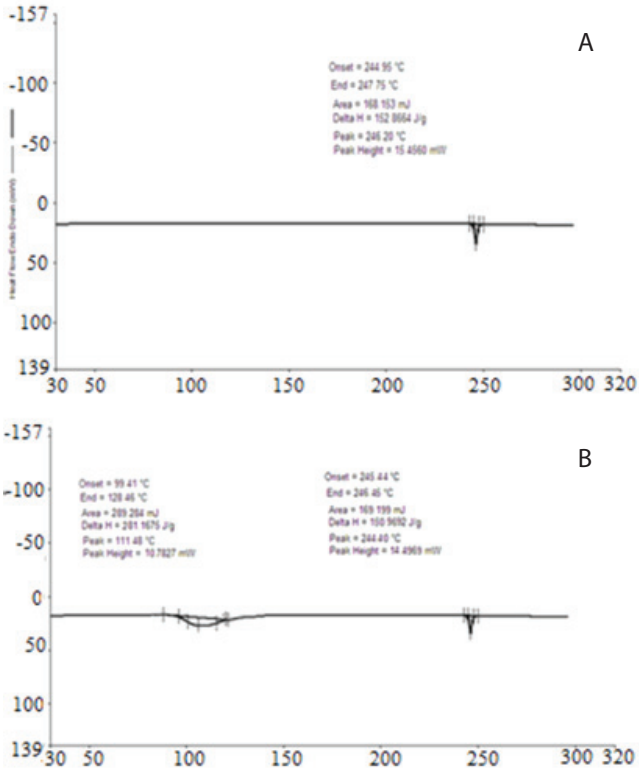

Fig. 4. Differential scanning calorimetry thermogram of (A) NVP and (B) NVP hydrotropic solid dispersion (lactose-citric acid)

Differential scanning calorimetry analysis

The DSC thermogram of NVP is shown in Fig. 3a. The DSC thermogram of NVP shows an endothermic melting peak at 246.20°C, indicating its melting point (244–247°C). The DSC thermogram of NVP solid dispersion is shown in Fig. 3b. There was no shift in the NVP endothermic peak; hence there was no NVP and excipient (lactose-citric acid) interaction. The separate endothermic peak of lactose was found at 111.4°C due to its dehydration.[39]

Conclusion

From the present research, we conclude that hydrotropy is an effective, safe and novel method to increase the solubility of poorly water-soluble drugs. Quick dissolution of the practically insoluble drug NVP in aqueous dissolution media indicates its potential to solubilize the drug in biological fluids, and thus significant enhancements in the onset of the effect and bioavailability can be seen. Therefore, the concept of mixed hydrotropy is an emerging field and greater importance must be given by the scientific community to explore its applicability and efficiency.

References

1. Dua K, Ramana MV, Sara UV, et al. Investigation of enhancement of solubility of norfloxacin beta-cyclodextrin in presence of acidic solubilizing additives. *Curr Drug Deliv.* 2007;4(1):21–25.
2. Gorajana A, Rajendran A, Yew LM, Dua K. Preparation and characterization of cefuroxime axetil solid dispersions using hydrophilic carriers. *Int J Pharm Investig.* 2015; 5:171–178.
3. Kumar N, Jain AK, Singh C, Agarwal K, Nema RK. Development, characterization and solubility study of solid dispersion of terbinafine hydrochloride. *Int J Pharm Sci Nanotech.* 2008;1:171–176.
4. James K. Solubility and related properties. Vol. 28, Marcel Dekker, New York, 1986, 127–146, 355–395.
5. Aulton ME. *Pharmaceutics – The Science of Dosage Form Design*. 2nd Ed, Harcourt Publishers Limited; 2002.
6. Waterbeemed HVD, Testa B. Drug bioavaibility; estimation of solubility, permeability, absorption. Wiley Online Library. 2009.
7. United State Pharmacopoeia XXI – NF XVI. Rockville, MD: United States Pharmacopeial Convention; 1985:1336.
8. Aggarwal S, Gupta GD, Chaudhary S. Solid dispersion as an eminent strategic approach in solubility enhancement of poorly soluble drugs. *Int J Pharma Sci Res.* 2010;1:1–13.
9. Bauduin P, Renoncourt A, Kopf A, Touraud D, Kunz W. Unified concept of solubilization in water by hydrotropes and co solvents. *Langmuir.* 2005;21:6769–6775.
10. Dhapte V, Mehta P. Advances in hydrotropic solutions: An updated review. *St. Petersburg Polytechnic Univ J Phys Math.* 2015;1:424–435.
11. Madan JR, Pawar KT, Dua K. Solubility enhancement studies on lurasidone hydrochloride using mixed hydrotropy. *Int J Pharm Invest.* 2015;5:114–120.
12. Kumar A, Sahoo AK, Padhee K, Pal P, Singh K. Review on Solubility Enhancement Techniques for Hydrophobic Drugs. *Int J Comprehensive Pharm.* 2011;3(3):1–7.
13. Elder DP, Holm R, Diego HL. Use of Pharmaceutical Salts and Cocrystals to Address the Issue of Poor Solubility. *Int J Pharm.* 2013;453:88–100.
14. Miyako Y, Khalef N, Matsuzaki K, Pinal R. Solubility enhancement of hydrophobic compounds by cosolvents: Role of solute hydrophobicity on the solubilization effect. *Int J Pharm.* 2010;393:48–54.
15. Kim J, Kim S, Papp M, Park K, Pinal R. Hydrotropic solubilization of poorly water soluble drugs. *J Pharm Sci.* 2010;9:53–65.
16. Pawar AR, Choudhari PD. Novel techniques for solubility, dissolution rate and bioavailability enhancement of class II and IV drugs. *Asian J Biomed Pharma Sci.* 2012;13(2):9–14.
17. Kumar A, Sahoo AK, Padhee K, Pal P, Singh K. Review on solubility enhancement techniques for hydrophobic drugs. *Int J Comprehensive Pharm.* 2011;3(3):1–7.
18. Limbachiya MI, Agarwal M, Sapariya A, Soni S. Solubility enhancement techniques for poorly soluble drugs: Review. *Int J Pharm Res Develop.* 2011;4(4):71–86.
19. Jatwani S, Rana AC, Singh G, Aggarwal G. An overview on solubility enhancement techniques for poorly soluble drugs and solid dispersion as an eminent strategic approach. *Int J Pharm Sci Res.* 2012;3(4):942–956.
20. Sikarra D, Shukla V, Kharia AA, Chatterjee DP. Techniques for solubility enhancement of poorly soluble drugs: An overview. *J Med Pharm Allied Sci.* 2012;1:1–22.
21. Gorajana A, Kit WW, Dua K. Characterization and solubility study of norfloxacin-polyethylene glycol, polyvinylpyrrolidone and carbopol 974P solid dispersions. *Recent Pat Drug Deliv Formul.* 2015;9(2):167–182.
22. Behera AL, Sahoo SK, Patil SV. Enhancement of solubility: A pharmaceutical overview. *Der Pharmacia Lettre.* 2010;2(2):310–318.
23. Saleh AM, El-Khordagui LK. Hydrotropic agents: A new definition. *Int J Pharm.* 1985;24:231–238.
24. Yalkowsky SH. *Solubility and solubilization in aqueous media*. New York, NY: Oxford University Press; 1999.
25. Leuenberger H. Spray freeze-drying – the process of choice for low water soluble drugs? *J Nanopart Res.* 2002;4:111–119.
26. Madan JR, Kamate VJ, Awasthi R, Dua K. Formulation, characterization and *in-vitro* evaluation of fast dissolving tablets containing gliclazide hydrotropic solid dispersions. *Recent Pat Drug Deliv Formul.* 2017; [E-pub ahead of print].
27. Awasthi R, Kulkarni GT. Development and characterization of amoxicillin loaded floating microballoons for the treatment of *Helicobacter pylori* induced gastric ulcer. *Asian J Pharm Sci.* 2013;8:174–180.
28. Dhiman N, Awasthi R, Jindal S, Khatri S, Dua K. Development of bilayer tablets with modified release of selected incompatible drugs. *Polim Med.* 2016;46(1):5–15.
29. Das P, Kumar K, Nambiraj A, Awasthi R, Dua K, Himaja M. Potential therapeutic activity of *Phlogacanthus thyrsiformis* Hardow (Mabb) flower extract and its biofabricated silver nanoparticles against chemically induced urolithiasis in male Wistar rats. *Int J Biol Macromol.* 2017;103:621–629.
30. Ramana MV, Dua K, Awasthi R. Development and characterization of solid dispersion-microsphere controlled release system for poorly water soluble drug. *Drug Deliv Trans Res.* 2016;6(5):540–550.
31. Lyn LY, Sze HW, Rajendran A, Adinarayana G, Dua K, Garg S. Crystal modifications and dissolution rate of piroxicam. *Acta Pharm.* 2011;61:391–402.
32. Dua K, Pabreja K, Ramana MV, Lather V. Dissolution behavior of β-cyclodextrin molecular inclusion complexes of aceclofenac. *J Pharm Bioallied Sci.* 2011;3(3):417–425.
33. Ramkumaar GR, Srinivasan S, Bhoopathy TJ, Gunasekaran S, Charles J, Ramesh J. Molecular structure, vibrational spectra, UV–vis, NBO, and NMR analyses on nevirapine using ab initio DFT methods. *J Theor Appl Phy.* 2013;7:51.
34. Sarkar M, Perumal OP, Panchagnula R. Solid-state characterization of nevirapine. *Ind J Pharm Sci.* 2008;70(5):619–630.
35. Inactive ingredient search for approved drug products. https://www.accessdata.fda.gov/scripts/cder/iig/getiigWEB.cfm. Published June 4, 2017. Updated July 5, 2017. Accessed July 20, 2017.
36. Maheshwari RK, Jagwani Y. Mixed Hydrotropy: Novel Science of Solubility Enhancement. *Indian J Pharm Sci.* 2011;73(2):179–183.
37. Zidan AS, Rahman Z, Sayeed V, Raw A, Yu L, Khan MA. Crystallinity evaluation of tacrolimus solid dispersions by chemometric analysis. *Int J Pharm.* 2012;23:341–350.
38. Newman A, Knipp G, Zografi G. Assessing the performance of amorphous solid dispersions. *J Pharm Sci.* 2012;101:1355–1377.
39. Raut DM, Allada R, Pavan KV. Dehydration of Lactose Monohydrate: Analytical and Physical Characterization. *Der Pharmacia Lettre.* 2011;3(5):202–212.

Light-cured dimethacrylate dental restorative composites under a prism of annihilating positrons

Olha Shpotyuk[1,A–D,F], Adam Ingram[2,B,C,E], Oleh Shpotyuk[3,C,E,F], Elvira Bezvushko[1,A,C,E,F]

[1] Department of Pediatric Dentistry, Danylo Halytsky Lviv National Medical University, Ukraine
[2] Department of Physics, Opole University of Technology, Poland
[3] Institute of Physics, Jan Długosz University in Częstochowa, Poland

A – research concept and design; B – collection and/or assembly of data; C – data analysis and interpretation;
D – writing the article; E – critical revision of the article; F – final approval of the article

Polymers in Medicine, ISSN 0370-0747 (print), ISSN 2451-2699 (online) *Polim Med.* 2017;47(2):91–100

Address for correspondence
Oleh Shpotyuk
E-mail: olehshpotyuk@yahoo.com

Funding sources
none declared

Conflict of interest
none declared

Received on July 25, 2017
Reviewed on December 4, 2017
Accepted on December 21, 2017

Abstract

Background. Breakthrough resolutions in current biopolymer engineering rely on reliable diagnostics of atomic-deficient spaces over the finest sub-nanometer length scales. One such diagnostic is positron annihilation lifetime spectroscopy, which probes space-time continuum relationships for the interaction between electrons and their antiparticle (positrons) in structural entities like free-volume defects, vacancies, vacancy-like clusters, interfacial voids and pores, etc.

Objectives. This paper is intended to highlight the possibilities of positron annihilation lifetime spectroscopy as an informative instrumentation tool to parameterize free-volume evolution in light-cured dimethacrylate dental restorative composites exemplified by Charisma® (Heraeus Kulzer GmbH, Hanau, Germany) and Dipol® (Oksomat-AN Ltd, Kyiv, Ukraine).

Material and methods. The subjects of the study were the commercially available dimethacrylate-type dental restorative composites Charisma® and Dipol®. The analysis used a fast-fast coincidence system of 230 ps resolution based on 2 photomultiplier tubes coupled to BaF_2 scintillator detectors and ORTEC® (ORTEC, Oak Ridge, USA) electronics to register lifetime spectra in normal-measurement statistics evolving ~1 million coincidences.

Results. The annihilation process in both composites is identified as mixed positron-Ps (positronium) trapping, where ortho-Ps decaying is caused entirely by free-volume holes in the polymer matrix, and the 2nd component is defined mainly by interfacial free-volume holes between filler nanoparticles and the surrounding polymer. The most appropriate model-independent estimation of photopolymerization volumetric shrinkage in dental restorative composites can be done using averaged positron annihilation lifetime. Partially-constrained x4-term analysis of lifetime spectra is less efficient, giving greater scatter of variance with an additional artifact of fixed shortest lifetime allowing unresolved mixing in the 2nd component. A meaningful phenomenological description of transformations in Ps and positron-trapping sites under light curing, which occurs more efficiently in Charisma® than in Dipol® nanocomposites, can be developed at the basis of a semi-empirical model exploring a x3-x2-coupling decomposition algorithm.

Conclusions. A deep understanding of void-evolution processes in dimethacrylate dental composites employing positron annihilation lifetime spectroscopy makes it possible to diagnose, characterize and engineer novel biomaterials for advanced use in medical practice.

Key words: positron annihilation lifetime spectroscopy, dental restorative composites, light curing, dimethacrylate

DOI
10.17219/pim/81450

Introduction

Composite biomaterials based on dimethacrylate polymers are currently of strong interest to a great number of scientists in view of their practical medical applications, mainly as promising light-cured dental restoratives.[1,2] Today, in due course of the development of 3rd-generation biopolymers possessing such features as bioinertness, bioactivity and resorbability, it is of high importance to explore not only their atomic level of structural organization, but also the atomic-deficient or void-relevant level.[3] A necessity to provide highly reliable tools for the technological modification and exhaustive characterization of these structural levels, reaching extremely low nano- and subnanometer length scales, is a pivotal requirement to overall success in the engineering of advanced biocomposites.

One of the breakthrough resolutions of this problem seems to be the diagnostics of atomic-deficient space, which could be quite informative in measuring possibilities, despite the enormous variety in the chemistry of different biomaterials. Positron annihilation lifetime (PAL) spectroscopy is known to be an example of such void-sensitive structural methods.[4–9] This experimental technique, which probes space-time continuum determination for the interaction between electron e^- and its antiparticle (positron e^+), is especially sensitive to tiny atomic-deficient entities (like free-volume defects, vacancies, vacancy-like clusters and their complexes, interfacial voids and pores, intergranular boundaries, etc.), which are highly deterministic in the functionality of modern biopolymers, using the recent advantages of nanotechnology.[9,10] But hitherto, the PAL method has been applied mainly to "purely technical" materials, compounds and polymers, semiconductor and metallic alloys, etc.[4,7,8] The attempts to use this technique for composite biopolymers have not been very successful so far because of significant complications in the unambiguous interpretation of the obtained experimental data.

In this work, PAL spectroscopy will be comprehensively examined in application to 2 advanced dimethacrylate-based dental restorative composites (DRC), Charisma® (Heraeus Kulzer GmbH, Hanau, Germany) and Dipol® (Oksomat-AN Ltd, Kyiv, Ukraine), both possessing monomer matrices consisting of BisGMA (bisphenol A-glycidyl methacrylate) and TEGDMA (triethyleneglycol dimethacrylate) modified with a multisized filler having a highly dispersive phase of silica SiO_2 glass.[11,12]

Material and methods

Sample preparation details

The experimental PAL studies were performed for 2 types of commercially available dental restorative composites (DRC), i.e., Charisma® and Dipol®, which are similar from a structural-chemical point of view (both belonging to resin composites based on dimethacrylate-type polymeric networks), but somewhat different in respect to volumetric shrinkage. The DRC specimens studied were prepared by filling an inner volume of disc-shaped plastic molds of uniform size having 6 mm in diameter and 2 mm in thickness. The bottom end surface of the plastic disc was covered by polyethylene slice film, which was separated from the sample along with the outer ring around the disc before the PAL experiments. These batches of non-polymerized DRC samples were respectively marked as Dipol-0 and Charisma-0. Then, part of these DRC samples were polymerized by illuminating their upper surfaces with a standard curing dental wireless LED source (LED.T4, SEASKY, Beijing, China), which emitted light in a 420–480 nm spectral range with ~900 mW/cm^2 output power density. To normalize the light curing protocol for all DRC specimens, the end of the guide tip from the light source was maintained just above the sample surface at a distance of 7 mm, so that the curing light beam fully covered the sample surface. The overall polymerization duration with this LED source was 60 s to ensure the deeply polymerized state of each DRC (in accordance with manufacturers' instructions).[11,12] The photopolymerized DRC batches (5 plate samples in A3 shade separated from the disc-shaped plastic molds) were marked as Dipol-60 and Charisma-60. The DRC specimens were stored dry at room temperature (~20°C) for 3 days prior to being used in the PAL measurements.

Positron annihilation lifetime spectra measurement

The experimental PAL spectra were registered with a fast-fast coincidence system of 230 ps resolution based on 2 Photonis XP2020/Q photomultiplier tubes coupled to BaF_2 scintillator 25.4A10/2M-Q-BaF-X-N detectors (Scionix, Bunnik, Holland) and ORTEC® electronics (ORTEC, Oak Ridge, USA). To ensure the most reliable measurements, which is a pre-condition of correct decomposition, each PAL spectrum was recorded at T = 22°C and a relative humidity of 35% in normal-measurement statistics reaching nearly 1 million coincidences. The channel width of 6.15 ps allowed 8000 channels in total. The radioactive ^{22}Na isotope of low ~50 kBq activity prepared from aqueous solution of ^{22}NaCl wrapped by Kapton® foil (DuPont™, Circleville, USA) of 12 μm thickness and sealed was used as the source of positrons sandwiched between the 2 tested samples.

The measured PAL spectra were processed with the LT 9.0 program,[13] stabilizing an average positron lifetime τ_{av}^{Σ} as the center of mass of the full PAL spectrum:

$$\tau_{av}^{\Sigma} = \sum_i I_i \tau_i \qquad (1)$$

where τ_i and I_i denote the positron lifetime and intensity of the corresponding fitting components (the resultant accuracies in lifetime and intensity determination were ±0.005 ns and ±0.5%, respectively).

The best fitting of PAL spectra was achieved via mixed channels of trapping, occurring due to defect-related positron e^+ traps and bound positron-electron e^+-e^- (positronium Ps) states. This task can be solved due to multicomponent fitting of PAL spectra with 3 or 4 negative exponentials under unconstrained (free fitting components) or constrained (most often for some fixed fitting parameters, such as shortest positron lifetime maintained close to 0.125 ns)[14–16] decomposition procedures, and normalized component intensities (I = 3.4):

$$\sum_i I_i = 1 \tag{2}$$

Positron annihilation lifetime spectra treatment algorithms

Because of the repulsive interaction with nuclei of environment, the positron e+ penetrates intrinsic regions of preferentially negative-charged or neutral free-volume structural voids. Therefore, the fitting covers realistic channels caused by positrons e^+, which annihilate from delocalized states in defect-free bulk, and those trapped from spatially-extended free-volume defects (e^+ trapping) and bound e^+-e^- states through "pick-up" annihilation with an electron of surrounding material (Ps decaying).

The canonical 2-state trapping model with only 1 kind of e^+-trapping defect can be applied to parameterize the experimental PAL spectrum under the condition of a small contribution from the 3rd and higher components, i.e., ignoring all Ps decaying channels.[4,6–8] This process is characterized by mean lifetime for e^+-trapping $\tau_{av}{}^{tr}$, defect-free bulk lifetime τ_b, trapping rate in defects κ_d and fraction η of trapped e^+, defined in respect to the following equations:

$$\tau_{av.} = \frac{\tau_1 I_1 + \tau_2 I_2}{I_1 + I_2} \tag{3}$$

$$\tau_b = \frac{I_1 + I_2}{\frac{I_1}{\tau_1} + \frac{I_2}{\tau_2}} \tag{4}$$

$$\kappa_d = \frac{I_2}{I_1}\left(\frac{1}{\tau_b} - \frac{1}{\tau_2}\right) \tag{5}$$

$$\eta = \frac{\kappa_d}{\lambda_b + \kappa_d} = \frac{\kappa_d \tau_b}{1 + \kappa_d \tau_b} = \tau_1 \kappa_d \tag{6}$$

In addition to these e^+-trapping models, the difference between defect-related and defect-free lifetimes, $(\tau_2 - \tau_b)$ can be accepted as a signature of size of e^+ traps in terms of the equivalent number of vacancies, whereas the τ_2/τ_b ratio can be ascribed to the nature of these free-volume defects.[4] In fact, such a 2-state trapping model describes e^+ annihilating from 2 distinct states, these being lattice-delocalized and defect-localized states, ignoring back escape of trapped positrons.[4,6–8]

The Ps decaying forms another channel of the PAL spectrum, which is caused by e^+ annihilating from the Ps state as free particles or interacting with e^- from the environment.[4–6] In the ground state, the Ps exists as para-Ps (p-Ps, antiparallel e^--e^+ spins) decaying intrinsically with 2 γ-quanta and character lifetime in a vacuum of 0.125 ns, and ortho-Ps (o-Ps, parallel e^--e^+ spins) decaying with 3 γ-quanta and lifetime of 142 ns, these states being occupied with a relative formation rate of 1:3. Since e^+ wave function overlaps with e^- outside, the annihilation with such e^- having an antiparallel spin decreases their lifetime to 0.5–10 ns, resulting in 2 γ-rays ("pick-off" annihilation).[4,5] Two conditions should be satisfied to form Ps, the 1st being a sufficiently high radius of void captured Ps, and the 2nd being low electron density preventing direct e^+-e^- annihilation.[5] The Ps localized in free-volume spaces gives an indication of their mean radii R in terms of long-lived τ_3 lifetime (the relative intensity of this component I_3 correlates with the density of Ps sites) in respect to the Tao-Eldrup equation:

$$\tau_3 = 0.5 \cdot [1 - \frac{R}{R + \Delta R} + \frac{1}{2\pi} \cdot \sin(\frac{2\pi R}{R + \Delta R})]^{-1} \tag{7}$$

where ΔR = 0.166 nm is the fitted empirical layer thickness.[4,5]

By fitting the above equation with measured τ_3, the R_3 and corresponding free volumes V_f in spherical approximation can be determined. The fractional free-volume f_v can be calculated as:

$$F_v = C \cdot I_3 \cdot V_f \tag{8}$$

using the empirical constant C = 0.0018 Å^{-3}.[5]

Thus, in the case of highly-inhomogeneous substances such as polymers, molecular compounds or composites, the PAL spectra are expected to be composed through a mixed e^+-Ps-trapping path.

In case of stronger input from Ps decaying in the x3-term decomposed PAL spectrum (as for many nanocomposites[5,9,14–21]), the e^+-trapping can be defined in terms of a simple trapping model assuming 2 additive inputs arise from trapped e^+ and decayed o-Ps states.[22] This model with 2 additive e^+-trapping defects with κ_{d1} and κ_{d2} annihilation rates defined as

$$\kappa_{d1} = I_2\left(\frac{1}{\tau_1} - \frac{1}{\tau_2}\right) \tag{9}$$

$$\kappa_{d2} = I_3\left(\frac{1}{\tau_1} - \frac{1}{\tau_3}\right) \tag{10}$$

$$\tau_b = \left(\frac{I_1}{\tau_1} + \frac{I_2}{\tau_2} + \frac{I_3}{\tau_3}\right)^{-1} \tag{11}$$

Results and discussion

The raw PAL spectra were reconstructed from unconstrained x3-term and partially-constrained x4-term fitting procedures assuming the shortest lifetime τ_1 fixed at the theoretical value of intrinsic p-Ps self-annihilation (0.125 ns). These spectra are depicted at a general background of source contribution for initial and photopolymerized DRC in Fig. 1 and 2, respectively. The narrow-restricted statistical scatters of variance tightly grouped around the 0-axis testify that the PAL measurements are well described within these fitting procedures, but unconstrained x3-term decomposition has an obvious preference in view of better goodness of fit.

The best-fit parameters of the detected PAL spectra decomposed in 3 negative exponentials are given in Table 1. The numerical values of e^+-trapping and Ps-decaying modes for these DRC calculated with respect to the above formalism of equations (1)–(8) ignoring contribution from o-Ps decaying are presented in Table 2. The similar results obtained with equations (9)–(11) assuming 2 additive e^+-trapping defect states are summarized in Table 3, are given for the measured PAL spectra decomposed in 3 negative exponentials. The respective results for these PAL spectra reconstructed from partially-constrained x4-term analysis are gathered in Tables 4 and 5.

Numerous experiments during the recent decades testify that x3-term analysis is most commonly applied to reconstruct adequately raw PAL spectra for many inhomogeneous polymer/filler composites.[14–21] Under such analysis (arranged as constraint-free decomposition[14–20] or partially-constrained decomposition fixing the shortest τ_1 lifetime[14,15,21]), the 3rd component with a long-lived lifetime τ_3 is ascribed to o-Ps annihilation in free-volume holes (voids), the 2nd component with an intermediate lifetime τ_2 is due to free positron annihilation in interfacial free volumes or other defect states mainly in a solid phase, and the 1st component with the shortest lifetime τ_1 is attributed to p-Ps self-annihilation conjugated with reduced e^+ annihilation from defect-free bulk state.[4–6] The lifetime-fixing fitting is preferred to overcome inadequacy in the resolving of the shortest component due to mixing different annihilation events (especially, when I_1 intensity occurs to be substantially greater than I_3).[14,15] In such a case, the fixing τ_1 to the value of p-Ps lifetime improves the reliability of the finite-term analysis, not affecting the o-Ps lifetime.[14] Nevertheless, unconstrained x3-decomposition has some, albeit limited, physical rel-

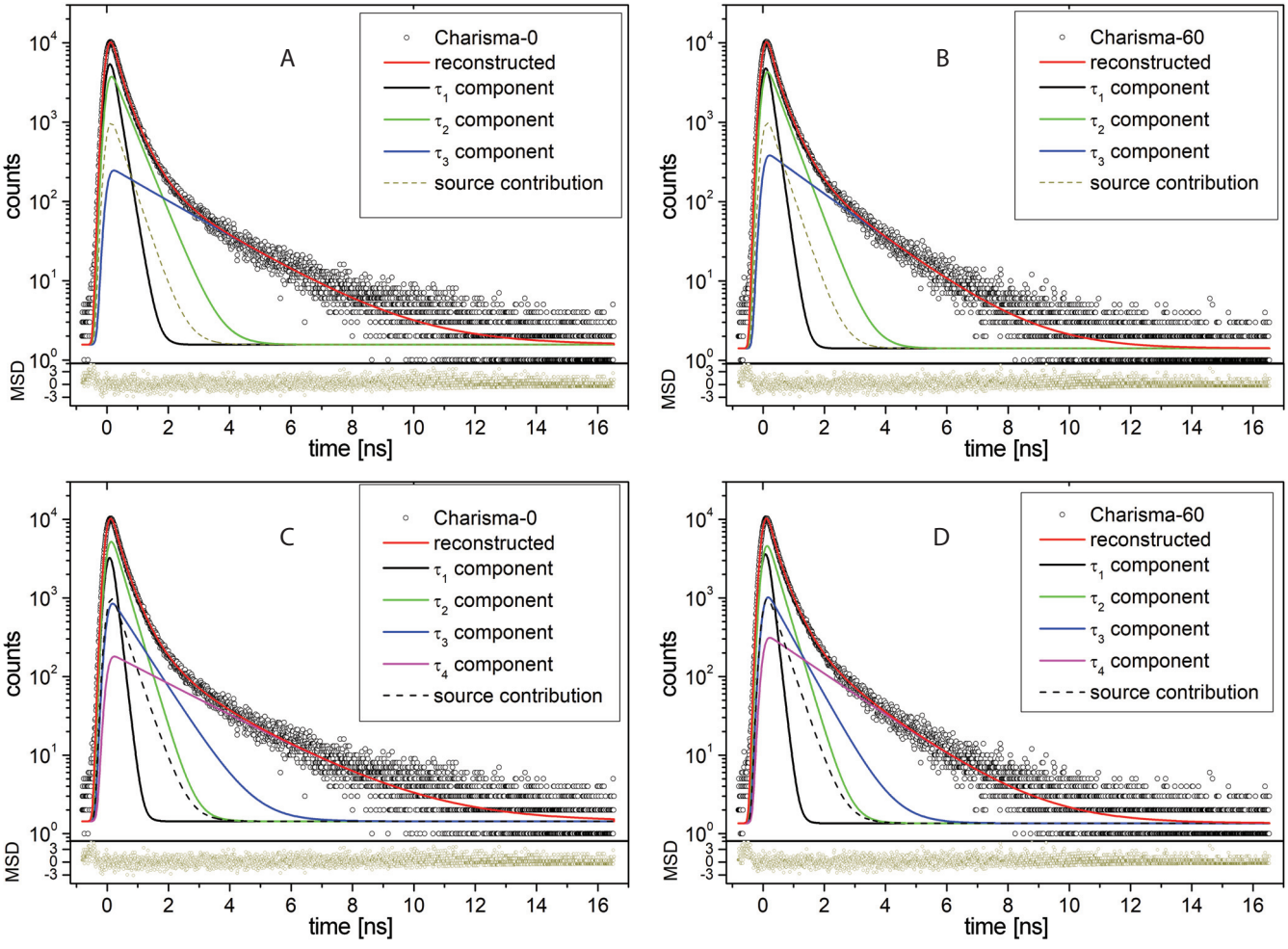

Fig. 1. Raw PAL spectra of non-polymerized Charisma-0 (A, B) and photopolymerized Charisma-60 (C, D) DRC reconstructed from unconstrained x3-fitting (A, C) and partially-constrained x4-fitting under fixed $\tau_1 = 0.125$ ns (B, D) at the background of source contribution (the bottom insets show statistical scatter of variance)

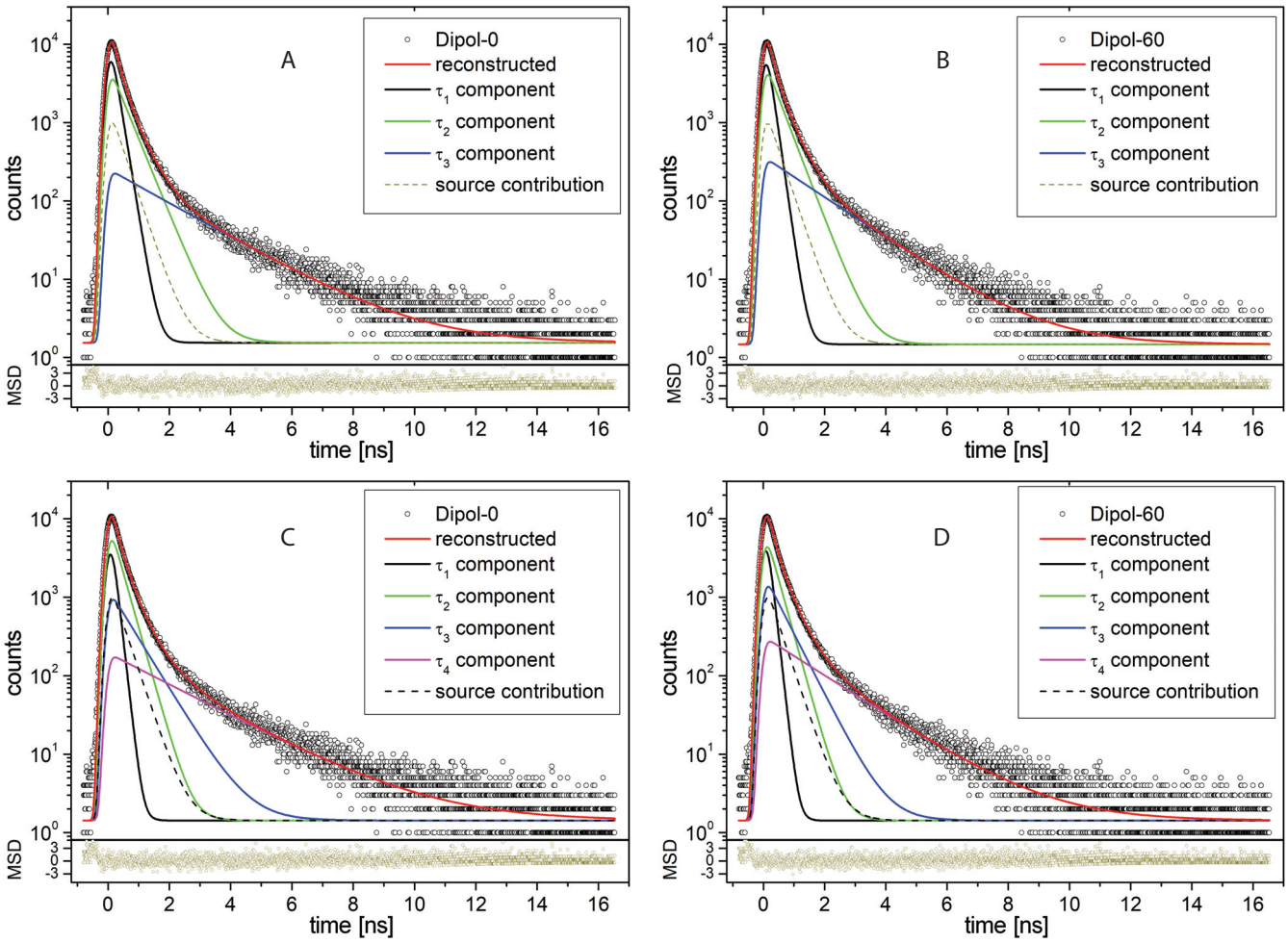

Fig. 2. Raw PAL spectra of non-polymerized Dipol-0 (A, B) and photopolymerized Dipol-60 (C, D) DRC reconstructed from unconstrained x3-fitting (A, C) and partially-constrained x4-fitting under fixed $\tau_1 = 0.125$ ns (B, D) in the background of source contribution (the bottom insets show statistical scatter of variance)

Table 1. PAL spectra fitting parameters for DRC within unconstrained x3-term decomposition

DRC	[FIT-1]	PAL spectra fitting parameters					τ_{av} [ns]
		τ_1 [ns]	τ_2 [ns]	τ_3 [ns]	I_2 [a.u.]	I_3 [a.u.]	
Dipol-0	0.038	0.178	0.444	1.978	0.510	0.085	0.466
Dipol-60	0.034	0.155	0.403	1.601	0.560	0.103	0.442
Charisma-0	0.020	0.179	0.447	1.946	0.540	0.092	0.486
Charisma-60	0.008	0.158	0.415	1.560	0.560	0.110	0.458

Table 2. PAL trapping models for DRC within unconstrained x3-term decomposition ignoring contributions from o-Ps decaying

DRC	e^+-trapping modes						Ps-decaying modes	
	τ_{av}^{tr} [ns]	τ_b [ns]	κ_d [ns^{-1}]	$\tau_2 - \tau_b$ [ns]	τ_2/τ_b [a.u.]	η [a.u.]	R_3 [nm]	f_v^3 [%]
Dipol-0	0.325	0.266	1.86	0.178	1.67	0.33	0.286	1.50
Dipol-60	0.309	0.251	2.45	0.152	1.61	0.38	0.248	1.17
Charisma-0	0.337	0.277	1.99	0.170	1.66	0.36	0.283	1.58
Charisma-60	0.321	0.260	2.50	0.155	1.60	0.40	0.243	1.19

evance allowing the most stable fitting.[14] Our previous results with some acrylic-type DRC also show that even under incomplete decomposition of the PAL spectra because of measuring instabilities, in part, in the vicinity of a 2nd component originated from free e^+ annihilation, the best goodness of reconstruction is achieved under constraint-free x3-fitting.[20] We also reconstructed the

Table 3. PAL trapping models for DRC within unconstrained x3-term decomposition assuming 2 additive positron-trapping defect states

DRC	τ_{av}^{tr} [ns]	τ_b [ns]	κ_{d1} [ns^{-1}]	κ_{d2} [ns^{-1}]
Dipol-0	0.466	0.288	1.72	0.43
Dipol-60	0.442	0.276	2.22	0.60
Charisma-0	0.486	0.302	1.81	0.47
Charisma-60	0.458	0.285	2.19	0.63

Table 4. PAL spectra fitting parameters for DRC within partially-constrained x4-term decomposition (τ_1 = 0.125 ns)

DRC	[FIT-1]	PAL spectra fitting parameters						τ_{av} [ns]
		τ_2 [ns]	τ_3 [ns]	τ_4 [ns]	I_2 [a.u.]	I_3 [a.u.]	I_4 [a.u.]	
Dipol-0	0.059	0.331	0.699	2.199	0.563	0.146	0.068	0.465
Dipol-60	0.093	0.310	0.560	1.746	0.483	0.208	0.085	0.442
Charisma-0	0.021	0.346	0.799	2.275	0.601	0.132	0.066	0.487
Charisma-60	0.069	0.327	0.615	1.670	0.530	0.169	0.092	0.457

Table 5. PAL trapping models for DRC within partially-constrained x4-term decomposition (τ_1 = 0.125 ns)

DRC	e^+-trapping modes						Ps-trapping modes			
	τ_{av}^{tr} [ns]	τ_b [ns]	κ_d [ns^{-1}]	$\tau_2 - \tau_b$ [ns]	τ_2/τ_b [a.u.]	η [a.u.]	R_3 [nm]	f_v^3 [%]	R_4 [nm]	f_v^4 [%]
Dipol-0	0.272	0.225	3.55	0.106	1.47	0.44	0.107	0.14	0.306	1.47
Dipol-60	0.251	0.211	3.26	0.099	1.47	0.41	0.063	0.04	0.263	1.17
Charisma-0	0.290	0.239	3.82	0.107	1.45	0.48	0.130	0.22	0.313	1.51
Charisma-60	0.270	0.224	3.55	0.103	1.46	0.44	0.082	0.07	0.255	1.15

PAL spectra with x3-decomposition procedure fixing the background input. The results of such PAL spectra treatment along with fit goodness (not shown in Table 1) occurred to be very similar to those obtained under constraint-free x3-fitting.

With respect to the PAL data parameterized within constraint-free x3-term analysis (Tables 1–3), the annihilation process in both DRC can be identified as mixed e^+-Ps-trapping, where "pure" o-Ps decaying is caused entirely by input from free-volume holes in the polymer matrix (3rd component), while the 2nd component is defined mainly by cumulative input from free e^+-trapping sites in a filler (including interfacial free-volume holes between filler particles/nanoparticles). Typical radii of o-Ps-trapping sites in the polymer matrix of the studied DRC estimated from equation (7) slightly differ, approaching 3 Å (2.86 Å in Dipol-0 and 2.83 Å in Charisma-0), the corresponding fractional free volumes f_v being 1.50% for Dipol-0 and 1.58% Å for Charisma-0 DRC (Table 2). The same applies to e^+-trapping channel defined by defect-related lifetimes close to $\tau_2 \cong 0.45$ ns. However, strict parameterization of this channel in terms of a 2-state trapping model seems rather meaningless under essential input from o-Ps decays.[4,6–8] The more realistic values of defect-free bulk lifetime τ_b related to positron annihilation from the Bloch states can be extracted from a simple model assuming additive e^+-trapping inputs from trapped e^+ and decayed o-Ps states (with lifetimes τ_2 and τ_3 given in Table 1).[22] The calculated τ_b values (Table 3) occur to be nearly 10% overestimated compared to those presented in Table 2.

The Charisma® DRC is known to be composed of the finest filler particles of ~10 nm pyrogenic silica SiO_2 glass, which provide weight-packing density reaching 78%.[11] The Dipol® DRC is structurally more variable, being composed of the finest filler particles of 1–3 nm, but smaller weight-packing density (72%).[12] As a result, the overall mass center of the PAL spectrum in non-polymerized Dipol-0 is shifted ~20 ps left as compared to Charisma-0 (Fig. 3). In spite of possible differentiation in filler size distribution, especially with respect to coarse-grained fraction, and variability in the finest filler fraction, these factors do not notably influence the PAL spectra shown in Fig. 1 and 2. This provides evidence for a similar intrinsic void structure responsible for e^+- and Ps-trapping in these DRC. The numerical parameters of e^--Ps-trapping models in Charisma-0 and Dipol-0 DRC gathered in Table 2 and 3 can be accepted as a signature of their similar inner void structure, which concerns both the geometrical characteristics of free-volume voids (sizes of trapping sites) and their preferential chemical environment (composed of fine-grained SiO_2 glass in a BisGMA-TEGDMA-based matrix).

In contrast, the x4-term analysis of the PAL spectra could be ignored for both DRC, at least, in view of the worse best-fit goodness (compare the goodness of fitting (FIT-1) values in Tables 1 and 4). Nevertheless, this reconstruction procedure is often applied for some polymer/filler composites, especially when the basic polymer shows bifurcation in o-Ps lifetimes, as it occurs, for instance, in semi-crystalline polymers like polyethylene or polytetrafluoroethylene.[14,15] In this case, the 4th longest-lived component is ascribed to o-Ps pick-off annihilation in holes of amorphous structure (τ_4 ~2–4 ns), and the 3rd intermediate component is ascribed to o-Ps pick-off annihilation in interstitial free-volume voids of the crystalline phase (τ_3 ~1 ns). Therefore, in polytetrafluoroethylene-based composites filled with silica nanoparticles, the PAL spectra were well resolved in 4 discrete negative exponentials, but only the 4th longest component was ascribed to o-Ps annihilation in a polymer matrix.[23]

Four discrete components were also resolved in the PAL spectra of some light-cured DRC based on dimethacrylate resins in other studies.[24–26] Within a x4-fitting route assuming fixed τ_1 value, the 4th component was ascribed to o-Ps annihilation in the main part of the polymer matrix, while the 3rd was explained as arising from o-Ps annihilation in the filler-matrix interphase. With re-

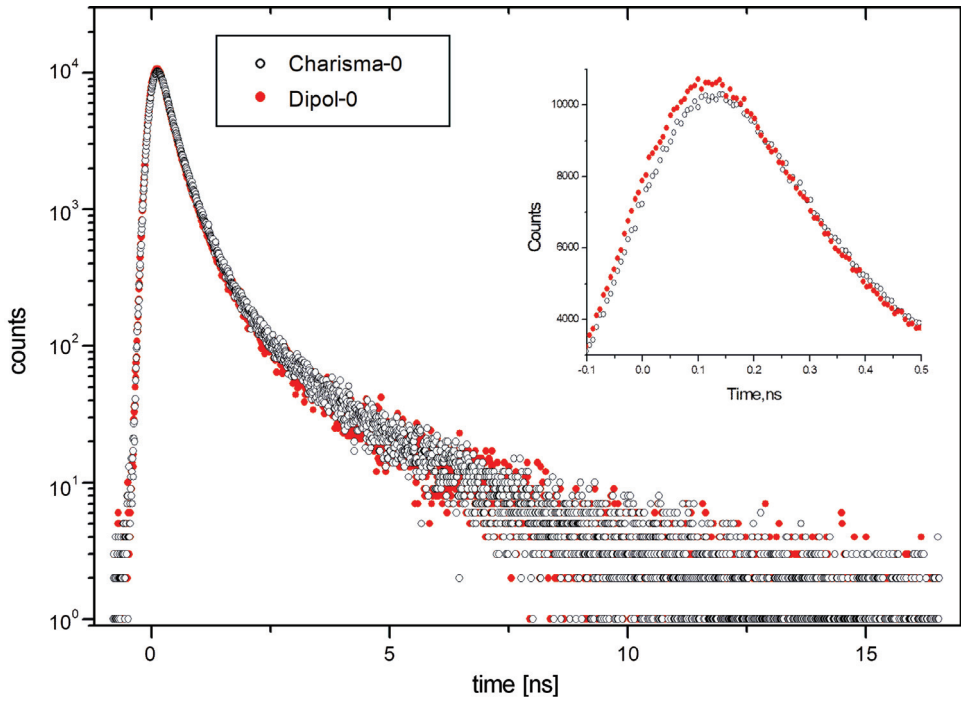

Fig. 3. Raw PAL spectra of non-polymerized Charisma-0 DRC as compared to that of Dipol-0 DRC (the inset shows a comparison of annihilation events accumulated in a peak)

spect to the latter, such an interpretation contradicts previous research, showing that only the 2nd component with 0.3–0.5 ns lifetime (free e^+ annihilation) is responsible for trapping in interfacial free volumes.[16–19] Recently, some current authors have shown that x4-fitting assuming fixed shortest lifetime (τ_1 = 0.125 ns) was also favorable for dimethacrylate DRC subjected to long-term aging, which were initially characterized by x3-decomposed best-fitted PAL spectra.[20,27] The origin of the additional component in o-Ps decaying in these polymer/filler DRC was not clarified unambiguously, while a version on stress-inducing destruction through growing inner and surface cracks seems quite plausible. It should be stressed that x4-term fitting parameters for Dipol® DRC affected by prolonged dry aging in the study mentioned above and non-polymerized Charisma-0 DRC in this research (Table 4) are very similar to the parameters for homemade DRC "Composite 16" in other studies.[20,24,25] Of note, all these DRC possess a polymer matrix of high crosslink density composed of a mixture of BisGMA and TEGDMA monomers.

In cases above, simple physical mixing in the 2nd component of x4-term decomposed PAL spectra due to interfacial holes and other alternatives (free-volume defects in the solid/polymer phase) cannot be excluded in separation separating the most realistic annihilation channels. This analysis may provide invalid parameterization of the 2nd component as an artifact of the inadequate x4-fitting route, since the polymer matrices of DRC based on bisphenol A polycarbonates are solely characterized by x3-term PAL spectra, where only a long-lived component comes undoubtedly from o-Ps decaying.[28–30] In the case of multiple o-Ps decays of the same origin, this component can be easily replaced by apparent lifetime, which is a mean value averaged over all o-Ps components with corresponding intensities.[30]

The most essential difference concerns the photopolymerization effect on the PAL trapping modes, revealed in the modulation depth for initial (non-cured) and final (light-cured) DRC.

Due to structural variability in the finest filler fraction, Dipol® DRC is known to possess relatively small photopolymerization volumetric shrinkage of 2.2%, while in Charisma® DRC this macroscopic parameter approaches 2.9%.[11,12] Thus, the volumetric shrinkages in these DRC are respectively rationed as ~1.3. Despite the eventual difference in the selectivity of the PAL method to different e^+-Ps trapping sites (not only those which determine macroscopic shrinkage), we suggest estimating this ratio based on free-volume void parameters extracted from x3-term PAL data (Table 2 and 3).

Thus, with respect to o-Ps trap sizes determined from τ_3 lifetime using equation (7), the spherical void volume in Dipol® DRC drops by 34.8% (from 93.6 Å^3 to 61.0 Å^3). In Charisma® DRC, this decrease is deeper, reaching nearly 40% (from 90.7 Å^3 to 54.4 Å^3). Thus, the corresponding ratio is close to 1.15. A similar value (1.12) can be obtained from photopolymerized dropping in fractional free volumes f_v. Therefore, the o-Ps traps themselves do not cover the overall macroscopic shrinkage in the studied DRC.

The similar calculations for a "pure" e^+-trapping channel defined from the 2nd component in the x3-term PAL spectra has no strong physical meaning, provided essential input from the 3rd component (related to o-Ps decaying).[4,5] Nevertheless, we shall perform such an estimation

ignoring this specificity, which can be admitted under a supposition on similar disturbance in the e^+-trapping channel from o-Ps traps in both DRC samples. Thus, the decrease in defect-related τ_2 lifetime (which reflects the size of respective e^+ traps) reaches 9.2% in Dipol® (from 0.444 ns to 0.403 ns; Table 2) and 7.2% in Charisma® (from 0.447 ns to 0.415 ns), giving an opposite effect in comparison, reaching ~0.8.[4–6] Such inconsistency is quite understandable in view of inadequacy in the interpretation of the 2nd component intensity I_2 in the x3-term decomposed PAL spectrum (which does not reflect solely the content of "pure" e^+ traps, but also balancing in the mixed e^+-Ps-trapping channels as a complement to full intensity normalization). Indeed, in contrast to a polymerization-induced decrease in fractional free-volume f_v for o-Ps, the fraction η of trapped e^+ reveals an enormous compensating increase of 15.2% in Dipol® (0.33–0.38; Table 2) and 11.1% in Charisma® DRC (0.36–0.40), thus giving it a ratio ~0.7.

Under a condition of mixed e^+-Ps-trapping channels, especially when these channels are inter-connected, the most adequate estimation of volumetric shrinkage independently of the computer-fitting procedure can be done using average $\tau_{av.}$ lifetime, e.g., mass center of PAL spectrum defined with respect to equation (1). As it is shown in Table 1, the light-curing results in $\tau_{av.}$ decrease, this effect reaching 5.1% for Dipol® (from 0.466 to 0.442 ns) and 5.8% for Charisma® DRC (from 0.486 to 0.458 ns). These values give ~1.2 in ratio, which can be accepted as being in very good accord with a rougher macroscopic estimation (~1.3).

Due to the trapping parameters defined from unconstrained x3-term decomposition (Table 1–3), the photopolymerization volumetric shrinkage in the DRC is well revealed through a decrease in average positron lifetime $\tau_{av.}$, this effect being accompanied by changes in both o-Ps- and e^+-trapping channels. Indeed, the photopolymerized DRC possess reduced long-lived lifetimes τ_3, but increased I_3 intensities (Table 1), thus resulting in smaller fractional free volumes f_v (Table 2). These changes are dominated in a light-cured state, being partially overbalanced by increased fraction η of trapped e^+ (Table 2), resulting from higher I_2 intensities and slightly suppressed τ_2 lifetimes (Table 1). The observed changes in o-Ps-trapping models can be ascribed preferentially to cross-linking of structural chains dominated in a "pure" polymer matrix, like it occurs in other polymers under UV light exposure, vulcanization (due to thermal curing) or γ-irradiation.[31–33] In fact, this causes a greater number of smaller voids in the photopolymerized DRC, thereby resulting in free-volume fragmentation for both existing o-Ps- and e^+-trapping sites, as illustrated by the schematic cartoon in Fig. 4. This global fragmentation trend can be well revealed in the increased trapping rates κ_{d1} and κ_{d2} for both DRC Dipol-60 and Charisma-60, defined within unconstrained x3-term fitting assuming 2 additive positron-trapping states arise from distinguished e^+- and Ps-trapping channels (Table 3).

By assuming that modification changes in o-Ps and e^+-trapping sites under light curing are mutually interconnected, so that no effects occur in other annihilation channels (such as annihilation from defect-free bulk states, or generation of novel Ps- or e^+ traps), we can treat the data within a x3-x2-coupling decomposition algorithm.[34,35] This approach concerns unconstrained x3-term reconstructed PAL spectra transformed to generalized x2-term form for host (non-polymerized) and modified (light-cured or photopolymerized) DRC, where a 2nd component involves contributions from all possible trapping inputs (e.g., e^+ traps, input from o-Ps decaying and p-Ps self-annihilation). Such simplification makes it possible to resolve additional components in the generalized x2-term PAL spectrum for modified matrix (with lifetime τ_{int} and intensity I_{int}), the compensating (τ_n, I_n) input in the 1st channel being found assuming a reasonable condition of full inter-channel equilibrium.[33–37] Thereby, the parameterization of transformed Ps-e^+ traps in the photopolymerized DRC matrix can be performed accepting (τ_n, I_n) and (τ_{int}, I_{int}) as the respective 1st and 2nd components of the generalized x2-term PAL spectrum for some hypothetical medium obeying parameterization, with respect to formalization of a simple 2-state positron-trapping model.[4–8] The defect-related τ_{int} positron lifetime in this model reflects appearing/disappearing traps in dependence on a positive/negative sign of I_n and I_{int} intensities.

The calculated trapping parameters of the studied light-cured DRC determined with respect to non-polymerized ones using the x3-x2-coupling decomposition algorithm are given in Table 6.[34,35] The negative I_n and I_{int} intensities testify that the parameterization concerns disappearing traps, which are rather like o-Ps free-volume holes with respect to τ_{int} values (0.656 ns for Charisma-60 and 0.768 ns for Dipol-60 DRC), exceeding the character level of o-Ps and p-Ps self-annihilation in a vacuum (0.5 ns).[4,5]

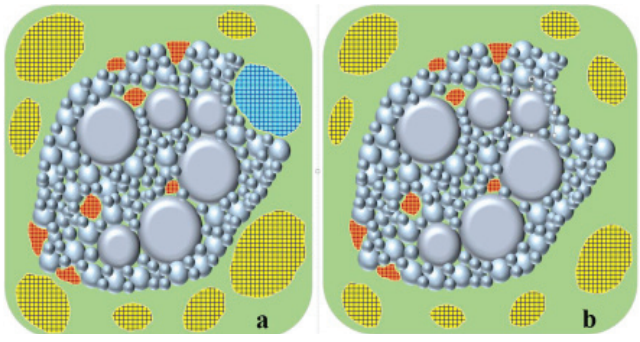

Fig. 4. Schematic cartoon showing fragmentation of free-volume Ps and e^+-traps in light-cured DRC: a – microstructure fragment of agglomerated filler particles (grey-colored) in non-polymerized DRC matrix (green-colored) containing o-Ps-trapping void located in interfacial filler-polymer region (blue-cross-dashed), o-Ps-trapping holes preferentially in polymer matrix (yellow-cross-dashed) and e^+-trapping sites preferentially in filler matrix (red-cross-dashed); b – the same agglomerate of filler particles in fully polymerized DRC matrix (o-Ps-trapping void in the interfacial filler-polymer region disappears, giving rise to more contracted o-Ps-trapping holes in surrounding polymer matrix and reduced trapping sites within agglomerated filler particles).

Table 6. PAL trapping models for light-cured DRC determined within x3-x2-coupling decomposition algorithm[34,35]

DRC	1st component		2nd component		Trapping modes		
	τ_n [ns]	I_n [a.u.]	τ_{int} [ns]	I_{int} [a.u.]	τ_{av} [ns]	τ_b [ns]	κ_d [ns^{-1}]
Charisma-60	0.409	–0.027	0.656	–0.086	0.597	0.573	0.70
Dipol-60	0.542	–0.018	0.768	–0.056	0.713	0.698	0.41

These traps are located preferentially at the grain boundaries of agglomerated filler particles (i.e., in the interfacial filler-polymer region possessing lower space occupation, Fig. 4a), as it follows from the sufficiently high defect-free bulk positron lifetime τ_b in Table 6 (0.597 ns for Charisma-60 and 0.713 ns for Dipol-60 DRC). In the due course of photopolymerization, these interfacial Ps-trapping sites disappear, giving rise to more contracted Ps traps (free-volume holes) in the surrounding polymer matrix and reduced trapping sites within agglomerated filler particles (Fig. 4b).

Conclusions

The characterization possibilities of positron annihilation lifetime spectroscopy are analyzed as they apply to 2 commercially available dimethacrylate-type dental restorative composites, Charisma® and Dipol®, both based on a monomer matrix consisting of bisphenol A-diglycidyl dimethacrylate (BisGMA) and triethylene glycol dimethacrylate (TEGDMA) modified with multisized filler particles having a highly dispersive phase of silica glass. These composites were studied in the initial and deeply light-cured states, using a conventional fast-fast coincidence positron lifetime spectrometer equipped with ORTEC® electronics. The PAL spectra were reconstructed from unconstrained x3-term and partially-constrained x4-term fitting routes, assuming the shortest lifetime fixed at a theoretical value of intrinsic para-Ps self-annihilation (0.125 ns).

With respect to the data parameterized within free x3-term analysis, the annihilation in the composites is identified as mixed positron-Ps trapping, where o-Ps decaying is caused entirely by free-volume holes in the polymer matrix, and the 2nd component is defined mainly by interfacial free-volume holes between the filler particles and surrounding polymer. Typical radii of o-Ps-trapping sites in a composite polymer matrix slightly differ, approaching 3 Å, and fractional free volumes reach 1.50% for Dipol® and 1.58% Å for Charisma®. The partially-constrained x4-term analysis of lifetime spectra is less efficient, giving greater scatter of variance with an artifact of fixed shortest lifetime, allowing unresolved physical mixing in the 2nd component. The most adequate model-independent estimation of polymerization volumetric shrinkage in the studied composites under condition of mixed positron-Ps trapping can be done in terms of average positron lifetime. The meaningful description of transformations in Ps and positron-trapping sites under light curing, which occurs more efficiently in the Charisma® than in the Dipol® composites, can be developed on the basis of a semi-empirical model exploring x3-x2-coupling decomposition algorithm.[34,35]

References

1. Cramer NB, Stansbury JW, Bowman CN. Recent advantages and developments in composite dental restorative materials. *J Dent Res*. 2011;90:402–416.
2. Ferracane JL. Resin composite – state of the art. *Dent Mater*. 2011;27:29–38.
3. Rühle M, Dosch H, Mittemeijer EJ, Van de Voorde MH. *European White Book on Fundamental Research in Materials Science*. Stuttgart: Max-Planck-Institut für Metallforschung; 2002.
4. Krause-Rehberg R, Leipner H. *Positron Annihilation in Semiconductors: Defect Studies*. Heidelberg: Springer; 1999.
5. Jean YC. Positron annihilation spectroscopy for chemical analysis: A novel probe for microstructural analysis of polymers. *Microchem J*. 1990;42:72–102.
6. Shpotyuk O, Filipecki J. *Free Volume in Vitreous Chalcogenide Semiconductors: Possibilities of Positron Annihilation Lifetime Study*. Czestochowa, Poland: Ed. WSP; 2003.
7. Keeble DJ, Brossmann U, Puff W, Würschum R. Positron annihilation studies of materials. In: Kaufmann EN, ed. *Characterization of Materials*. Hoboken, NJ: John Wiley & Sons; 2012:1899–1925.
8. Tuomisto F, Makkonen I. Defect identification in semiconductors with positron annihilation: Experiment and theory. *Rev Mod Phys*. 2013;85:1583–1631.
9. Jean YC, Van Horn JD, Hung WS, Lee KR. Perspective of positron annihilation spectroscopy in polymers. *Macromolecules*. 2013;46:7133–7145.
10. Mitra SB, Wu D, Holmes BN. An application of nanotechnology in advanced dental materials. *J Am Dent Assoc*. 2003;34:1382–1390.
11. Charisma®. Scientific Information. Heraeus Kulzer GmbH, Hanau, Germany, http://pantelides-dental.gr/userfiles/files/CharismaScientificInformation.pdf. Accessed April 11, 2018.
12. Dipol®. Composite Universal. Instruction on using Dipol materials. Oksomat-AN, Ukraine Dental Products, 6–7.
13. Kansy J. Microcomputer program for analysis of positron annihilation lifetime spectra. *Nucl Instrum Methods Phys Res A*. 1996;374:235–244.
14. Dlubek G, Clarke AP, Fretwell HM, Dugdale SB, Alam MA. Positron lifetime studies of free volume hole size distribution in glassy polycarbonate and polystyrene. *Phys Stat Sol*. 1996;A157:351–364.
15. Dlubek G, Saarinen K, Fretwell HM. Positron states in polyethylene and polytetrafluoroethylene: A positron lifetime and Doppler-broadening study. *Nucl Instrun Methods Phys Res B*. 1998;142:139–155.
16. Wang SJ, Wang CL, Zhu XG, Qi ZN. Structural characteristics of HDPE/CaCO3 polymer composites probed by positron annihilation. *Phys Stat Sol*. 1994;A142:275–280.
17. Zhang M, Fang PF, Zhang SP, Wang B, Wang SJ. Study of structural characteristics of HDPE/$CaCO_3$ nanocomposites by positrons. *Rad Phys Chem*. 2003;68:565–567.
18. Jia S, Zhang Z, Fan Y, Weng H, Zhang X, Hang R. Study of the size and numerical concentration of the free volume of carbon filled HDPE composites by the positron annihilation method. *Eur Polym J*. 2002;38:2433–2439.
19. Awad S, Chen HM, Grady BP, et al. Positron annihilation spectroscopy of polystyrene filled with carbon nanomaterials. *Macromolecules*. 2012;45:933–940.

20. Boyko O, Shpotyuk Y, Filipecki J. Positron annihilation lifetime study of extended defects in semiconductor glasses and polymers. *Phys Stat Sol C*. 2013;10:121–124.
21. Jobando VO, Quarles CA. Positron lifetime studies on the free volume changes during curing of rubber-carbon black composites. *Phys Stat Sol C*. 2007;4:3763–3766.
22. Liu M, Kitai AH, Mascher P. Point defects and luminescence centers in zinc oxide and zinc oxide doped with manganese. *J Lumin*. 1992;54:35–42.
23. Madami MM, MacQueen RC, Granata RD. Positron annihilation lifetime study of PTFE/silica composites. *J Polym Sci B*. 1996;34:2767–2770.
24. Kleczewska J, Bieliński DM, Dryzek E, Piątkowska A. Application of positron annihilation lifetime spectroscopy in studies of dental composites based on dimethacrylate resins. In: Pielichowski K, ed. *Modern Polymeric Materials for Environmental Application*. Vol. 4(1), Kraków, Poland: TEZA; 2010:143–150.
25. Kleczewska J, Bieliński DM, Ranganathan N, Sokołowski J. Characterization of light-cured dental composites. In: Ranganathan N, ed. *Materials Characterization. Modern Methods and Applications*. Boca Raton, FL: CRC Press Taylor & Francis Group; 2016:117–148.
26. Shirazinia M, Mehmandoost-Khajeh-Dad AA, Dehghani V, Mehmandoost-Khajeh-Dad J, Khaghani M. The effect of curing light intensity on free volume size in some dental composites. *Polim Med*. 2016;46:129–133.
27. Filipecki J, Chamerski K, Boyko O, Kotynia K. Ageing phenomenon in acrylic polymer dental materials detected by means of positron annihilation lifetime spectroscopy. *Polim Med*. 2014;44:21–28.
28. Pfeifer CS, Shelton ZR, Braga RR, Windmoller D, Machalo JC, Stansbury JW. Characterization of dimethacrylate polymeric networks: A study of the crosslinked structure formed by monomers used in dental composites. *Eur Polym J*. 2011;47:162–170.
29. Kluin JE, Yu Z, Vleeshouwers S, McGervey JD, Jamieson AM, Simha R. Temperature and time dependence of free volume in bisphenol A polycarbonates studied by positron lifetime spectroscopy. *Macromolecules*. 1992;25:5089–5093.
30. Kluin JE, Yu Z, Vleeshouwers S, et al. Ortho-positronium lifetime studies of free volume in polycarbonates of different structures: Influence of hole size distribution. *Macromolecules*. 1993;26:1853–1861.
31. Ramani R, Ranganathaiah C. Degradation of acrylonitrile-butadiene-styrene and polycarbonate by UV irradiation. *Polym Degrad Stab*. 2000;69:347–354.
32. Srithawatpong R, Peng ZL, Olson BG, et al. Positron annihilation lifetime studies of changes in free volume on cross-linking cis-polyisoprene, high-vinyl polybutadiene, and their miscible blends. *J Polym Sci B*. 1999;37:2754–2570.
33. Hyla M, Filipecki J, Swiatek J, Mervinskii RI. Gamma irradiation effects on UV-cured polymers based on acrylate oligomers studied by positron annihilation lifetime spectroscopy. *J Non-Cryst Solids*. 2005;351:1473–1476.
34. Shpotyuk O, Filipecki J, Ingram A, et al. Positronics of subnanometer atomistic imperfections in solids as a high-informative structure characterization tool. *Nanoscale Res Lett*. 2015;10:77–1–5.
35. Shpotyuk O, Ingram A, Filipecki J, Bujňáková Z, Baláž P. Positron annihilation lifetime study of atomic imperfections in nanostructurized solids: On the parameterized trapping in wet-milled arsenic sulfides As4S4. *Phys Stat Sol*. 2016;B253:1054–1059.
36. Shpotyuk O, Ingram A, Shpotyuk O. Free volume structure of acrylic-type dental nanocomposites tested with annihilating positrons. *Nanoscale Res Lett*. 2016;11:528–1–6.
37. Shpotyuk O, Adamiak S, Bezvushko E, et al. Light-curing volumetric shrinkage in dimethacrylate-based dental composites by nanoindentation and PAL study. *Nanoscale Res Lett*. 2017;12:75–1–6.

Formulation and evaluation of controlled-release matrix systems of ciprofloxacin

Venkata Ramana Malipeddi[1,A–F], Rajendra Awasthi[2,A–F], Kamal Dua[3,A–F]

[1] Amity Institute of Pharmacy, Amity University, Lucknow, India
[2] NKBR College of Pharmacy & Research Centre, Phaphunda, India
[3] Discipline of Pharmacy, Graduate School of Health, University of Technology Sydney, Australia

A – research concept and design; B – collection and/or assembly of data; C – data analysis and interpretation;
D – writing the article; E – critical revision of the article; F – final approval of the article

Polymers in Medicine, ISSN 0370-0747 (print), ISSN 2451-2699 (online) *Polim Med.* 2017;47(2):101–106

Address for correspondence
Venkata Ramana Malipeddi
E-mail: drmvramana@gmail.com

Funding sources
none declared

Conflict of interest
none declared

Received on August 27, 2017
Reviewed on December 18, 2017
Accepted on April 17, 2018

Abstract

Background. Ciprofloxacin is a broad-spectrum fluoroquinolone antibacterial drug to which most Gram-negative and many Gram-positive bacteria are highly susceptible. Fluoroquinolones are administered repeatedly, twice a day for 5 days, during the course of therapy. Hence, they require repeated administration. Ciprofloxacin qualifies as a drug candidate for a controlled-release drug delivery system.

Objectives. The present work was aimed to develop ciprofloxacin hydrochloride-containing matrix tablets by the wet granulation method.

Material and methods. The tablets were prepared using Ethocel™ 100 Premium and Eudragit® RS PO (Evonik Laboratory, Mumbai, India) as a rate-controlling polymer. Granular dioctyl phthalate (DCP) was used as a diluent. An isopropyl alcohol and dichloromethane (1:1) mixture was used as a granulating agent. The effect of the formulation variables on tablet performance was examined based on weight variation, hardness, friability, thickness, and drug release profiles. The results suggested that the tablets had good integrity.

Results. The tablets were stable for 18 months. Formulation F_7 gave a linear release pattern up to 12 h. The release of ciprofloxacin from formulation F_7 followed zero-order kinetics. The release mechanism was found to be diffusion-controlled as the Higuchi equation was obeyed.

Conclusions. Ciprofloxacin hydrochloride-containing matrix tablets were prepared successfully. The tablets had good integrity and were found stable for 18 months.

Key words: ciprofloxacin hydrochloride, diffusion-controlled, Ethocel™ 100 Premium, Eudragit® RS PO, matrix tablet

DOI
10.17219/pim/90020

Introduction

The rationale of designing an oral controlled release drug delivery system is to achieve a predetermined and reproducible drug release profile from the system.[1] Antibacterials are currently largely available on the market in the form of conventional dosage forms. Due to limitations in the use of conventional dosage forms, alternative dosage forms, such as sustained-release products, have been developed. Such products are available on the market only for a few drugs of these categories. Many antibacterials are still used in conventional dosage forms. There is a need to develop controlled-release drug delivery systems for these categories, so as to optimize the therapy and accrue the numerous benefits of controlled-release drug delivery systems. Antibiotics are substances produced by various species of microorganisms that suppress the growth of other microorganisms.[2] Common usage often extends the term "antibiotics" to include synthetic antimicrobial agents, such as sulfonamides and quinolones. The recent introduction of fluorinated 4-quinolones, such as ciprofloxacin and ofloxacin, represents an important therapeutic advance, since these agents have a broad antimicrobial activity and are effective after oral administration for the treatment of a wide variety of infectious diseases.[3] Peak serum levels are obtained within 1–3 h after administering an oral dose of 200 mg, with peak levels ranging from 0.7 μg/mL (sparfloxacin) to 2.9 μg/mL (trovafloxacin).[4] Fluoroquinolones are potent bactericidal agents against *Escherichia coli* and various species of *Salmonella*, *Shigella*, *Enterobacter*, *Campylobacter*, and *Niesseria*.[5]

Ciprofloxacin is a broad-spectrum fluoroquinolone antibacterial drug to which most Gram-negative bacteria and many Gram-positive bacteria are highly susceptible.[6] It has proven effective in the treatment of many types of systemic infections as well as acute and chronic infections of the urinary tract.[7] It is generally well tolerated; however, ciprofloxacin may produce nausea, vomiting, diarrhea, and abdominal discomfort after administration.[8] The gastric irritation and dose dumping problem of ciprofloxacin can be avoided by formulating a controlled-release drug delivery system. The oral dose of ciprofloxacin in adults is 500–750 mg for 12 h. The bioavailability of ciprofloxacin is 60–80%. The serum half-life for ciprofloxacin is 3.3 h. Fluoroquinolones are administered repeatedly, twice a day for 5 days, during the course of therapy. Hence, they require repeated administration.[9,10] Thus, ciprofloxacin qualifies as a candidate for a controlled-release drug delivery system.

To overcome the limitations of immediate release formulations of ciprofloxacin hydrochloride, the purpose of the present study was to design and develop matrix systems using Ethocel™ and Eudragit® RS PO as a solubility retardant to maintain a sustained release profile.

Material and methods

Material

Ciprofloxacin hydrochloride was received as a gift sample from Nicholas Piramal Ltd., Indore, India. Ethocel™ 100 Premium and Eudragit® RS PO were received as a gift sample from Evonik Laboratory, Mumbai, India. Granular dicalcium phosphate (DCP) was received as a gift sample from Dhara Life Science Pvt. Ltd., Ahmedabad, India. Microcrystalline cellulose (Avicel PH 112) was received as a gift sample from NB Entrepreneurs, Nagpur, India. Croscarmellose sodium (Ac-Di-Sol) was received as a gift sample from Signet Chemical Corporation, Mumbai, India. Isopropyl alcohol and dichloromethane were purchased from Thomas Baker (Chemicals) Pvt. Ltd., Mumbai, India. Sodium starch glycolate, microcrystalline cellulose, sodium lauryl sulfate, magnesium stearate, and purified talc were purchased from Nice Chemicals Ltd., Cochin, India.

Methods

Preparation of ciprofloxacin hydrochloride matrix tablets

Ciprofloxacin hydrochloride and a 75% amount of Ethocel 100 Premium and Eudragit RS PO were passed through #40 sieve and mixed thoroughly (Table 1). The remaining amount of the polymers was dissolved in 30 mL of an isopropyl alcohol and dichloromethane (1:1) mixture. The resultant solution was used as a binding agent to prepare a wet mass. The wet mass was passed through #12 sieve to form granules. The wet granules were dried in a hot air oven at 45 ±5°C for 1 h. The dried granules were passed through #20 sieve and mixed with the remaining ingredients previously passed through #40 sieve. The granules were lubricated and compressed using a 19.5 × 10 mm size punch (capsule shape) in a rotary tablet press (Rimek Mini Press 1; Karnavati Engineering Ltd., Ahmedabad, India).

Preparation of conventional ciprofloxacin hydrochloride tablets

The composition of the conventional tablets of ciprofloxacin is shown in Table 2. Ciprofloxacin hydrochloride, Avicel PH 112, sodium lauryl sulfate and Primojel® were passed through #40 sieve. Starch paste (10% w/w) was used as a binding agent. The wet mass was passed through #12 sieve and dried for 1 h. The dried granules were passed through #20 sieve. Lubricant and the other excipients were passed through #40 sieve and mixed with the dried granules for 5 min. The granules were compressed using a 16.4 × 8 mm size punch (capsule shape) in a rotary tablet press (Rimek Mini Press 1; Karnavati Engineering Ltd., Ahmedabad, India).

Table 1. Composition of the matrix tablets of ciprofloxacin hydrochloride (formulations F_1–F_9)

Ingredients	Quantity [mg/tablet]								
	F_1	F_2	F_3	F_4	F_5	F_6	F_7	F_8	F_9
Ciprofloxacin hydrochloride	580	580	580	580	580	580	580	580	580
Ethocel™ 100 Premium	100	150	200	–	300	300	300	–	–
Eudragit® RS PO	200	150	100	300	–	–	–	300	300
Granular DCP	60	50	40	40	40	50	60	50	60
Avicel PH 112	40	50	60	60	60	50	40	50	40
Magnesium stearate	10	10	10	10	10	10	10	10	10
Purified talc	10	10	10	10	10	10	10	10	10

DCP – dioctyl phthalate.

Table 2. Composition of a conventional tablet of ciprofloxacin hydrochloride (formulation F_{10})

Ingredients	Quantity [mg/tablet]
Ciprofloxacin hydrochloride	580
Microcrystalline cellulose	140
Sodium lauryl sulphate	10
Sodium starch glycolate (Primojel®)	27
Starch (for paste in water)	60
Ac-Di-Sol	15
Magnesium stearate	6
Purified talc	6
Purified water	q.s.

q.s. – quantum satis (enough).

Evaluation of tablets

The tablets produced were characterized for weight variation, hardness using a Monsanto hardness Tester (PI-924, Slit Lamp KFCO International, Ambala, India), friability using a friabilator meeting United States Pharmacopeia (USP) requirements (EF-2; Electrolab, Mumbai, India), and thickness using a Digital Vernier Caliper (500-197-20, Mitutoyo, Japan).[11,12] Each measurement was done in triplicate.

The release study of ciprofloxacin hydrochloride from the prepared tablets was carried out using USP dissolution apparatus II. The dissolution study was carried out in 900 mL of 0.1 N HCl (pH 1.2) for the initial 2 h and 900 mL phosphate buffer solution (PBS; pH 7.4) for the next 10 h at 100 rpm. The temperature was maintained at 37 ±0.5°C. Aliquots (5 mL) were withdrawn at every 1 h interval till the 12th h. The sink condition was maintained by replacing an equivalent amount of dissolution medium after each sampling. The samples were analyzed using a ultraviolet (UV) spectrophotometer (UV 3000$^+$; LabIndia Instruments, Mumbai, India) at 278 nm. The sampling was done in triplicate from each batch.[13]

To study the drug release behavior and kinetics, the dissolution data was fitted in various kinetic models viz. zero-order (cumulative amount of drug released against time) and first-order kinetics (log cumulative percentage of drug remaining against time). The drug release mechanism was investigated using Higuchi's model (cumulative percentage of drug released against the square root of time).[14]

Stability study

Stability studies on matrix tablets (formulations F_4, F_5 and F_7) were carried out according to the International Council for Harmonisation of Technical Requirements for Pharmaceuticals for Human Use (ICH) guidelines. Three tablets of each formulation were withdrawn, and observed visually for physical appearance (color or texture), drug content and dissolution profile at 0, 30th, 60th, 90th and 180th day. From the data, shelf life ($t_{90\%}$) was calculated.[15]

Results and discussion

Ciprofloxacin hydrochloride is water-soluble and it is rapidly and well absorbed from the gastrointestinal tract. The oral bioavailability of ciprofloxacin hydrochloride is 70%. Peak plasma concentration is obtained within 1–2 h and the plasma half-life of ciprofloxacin is 3–5 h. This results in rapid absorption and elimination of ciprofloxacin hydrochloride from a conventional tablet. In order to control the release of the drug, rate-retarding polymers, such as ethyl cellulose (Ethocel™ 100 Premium) and/or Eudragit® RS PO, were used in different proportions. Nine formulations (F_1–F_9) were prepared as matrix tablets with individual polymers and mixtures of the 2 polymers. For comparison, 1 formulation (F_{10}) was prepared by wet granulation method, using starch paste as a binding agent.

A spectrophotometric analytical method for ciprofloxacin was developed using distilled water as a solvent. The analytical wavelength of 278 nm was identified. The E1% solution gave 974. The molar extinction coefficient was 2.5×10^5. Beer-Lambert law was obeyed in the concentration range 1–10 μg/mL. The R2 value (0.9998) proved the validity of the analytical method used.

The granules were evaluated for percent moisture content. The moisture content was within acceptable limits. The tablets (formulations F_1–F_{10}) were evaluated for

physical integrity such as thickness, hardness, compressional weight, friability, and drug content. The results are presented in Table 3. The tablet surface was free of cracks and slumps. Weight variation is the major test to be checked frequently. Variation in the weight of the tablet leads to either undermedication or overdose. The average weight of the matrix tablets (formulations F_1–F_9) ranged from 980 to 1012 mg (expected weight of each tablet was 1000 mg). The weight of all tablets was within ±5% range of average weight. The average weight of the conventional tablet (formulation F_{10}) was 855 ±5 mg (expected weight was 844 mg).

Friability decreased as the binder concentration increased. An increase in binder concentration will enhance the formation of stronger inter-particulate bonds between the granules during compression. This means that the tablets would offer greater resistance to shock and abrasion since there is a stronger adhesive bonding of the granules at high binder concentrations. In general, tablets had good friability profiles (<0.8%).

The hardness of a tablet is an indication of its strength. The tablet should be stable to mechanical stress during handling and transportation. An increase in binder concentration increased the hardness of the tablets. Hardness of the tablets (formulations F_1–F_{10}) varied from 6.0 to 7.5 kg/cm^2. The hardness was satisfactory (5–10 kg/cm^2) (Table 3).

Tablets should have uniform thickness and these values are used to adjust the initial stage of compression. The thickness of the tablets (formulations F_1–F_9) varied from 6.2 to 6.5 mm, which is permissible as per the standards (usually a range of ±5% around the average thickness is allowed). The thickness of the conventional tablets (formulation F_{10}) ranged between 7.8 and 8.0 mm (Table 3). The thickness of all the formulations was found to be uniform.

The results showed that the disintegration time of the tablets increased from 5 ±0.17 to 11 ±0.52 min as the binder concentration increased from 0.25 to 1.0% (Table 3). The drug content was found to be in the range of 93.0–98.08%. The percentage moisture content of the granules at the time of compression (6.1–8.3%) was satisfactory for compression of the ciprofloxacin tablets. Drug content ranged from 96.4% to 96.6% of the expected drug content, which satisfies the compendial requirements. Thus, ciprofloxacin tablets with good physical integrity were obtained.

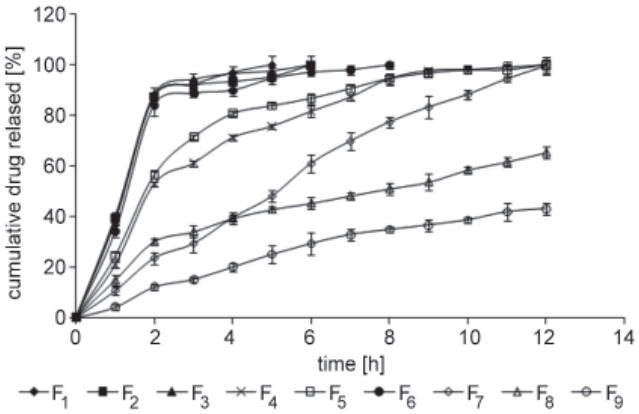

Fig. 1. In vitro release profile of ciprofloxacin hydrochloride from matrix tablets (formulations F_1–F_9) in 0.1 N HCl (pH 1.2) for initial 2 h and phosphate buffer solution (PBS) (pH 7.4) for the next 10 h at 37 ±0.2°C (mean ± SD, n = 3)

The in vitro release data of the 9 formulations (formulations F_1–F_9) are recorded in Fig. 1. Formulation F_{10} released 97.7% of the drug within 30 min of the dissolution study and was unsuitable for controlled release. The results of the in vitro release study indicated that the release of ciprofloxacin from 5 formulations (formulations F_1, F_2, F_3, F_6, and F_{10}) was very fast (>80% in 2 h). Hence, these formulations were not suitable for controlled release of ciprofloxacin. Formulations F_4, F_5, F_7, F_8, and F_9 gave a linear release pattern of ciprofloxacin up to 12 h. The release rate was slow and incomplete from formulation F_8 (63.35%) and F_9 (43.05%) after 12 h of dissolution study. Hence, formulations F_8 and F_9 were considered unsuitable for controlled release. Formulations F_4, F_5 and F_7 showed a continuous and complete release of ciprofloxacin up to 12 h (Fig. 1). A comparison of regres-

Table 3. Physical and chemical parameters of the matrix tablets of ciprofloxacin*

Parameter ↓	Formulations									
	F_1	F_2	F_3	F_4	F_5	F_6	F_7	F_8	F_9	F_{10}
Moisture content [% w/w]	7.40 ±1.03	7.30 ±0.57	6.90 ±0.65	7.30 ±0.97	6.87 ±1.51	5.93 ±0.85	6.50 ±1.06	6.00 ±0.96	5.69 ±1.13	6.10 ±0.82
Thickness [mm]	6.40 ±0.52	6.25 ±1.24	6.50 ±1.61	6.12 ±1.30	6.30 ±0.87	6.40 ±1.25	6.40 ±1.25	6.20 ±0.82	6.40 ±1.73	7.90 ±1.53
Hardness [kg/cm^2]	6.5 ±1.57	7.0 ±2.51	6.5 ±1.52	6.0 ±0.84	6.5 ±0.72	7.0 ±1.18	7.1 ±1.92	7.5 ±1.23	6.7 ±0.85	6.5 ±0.79
Compressional wt [mg] (practical)	990 ±5.39	987 ±7.64	992 ±5.95	980 ±6.91	997 ±5.86	984 ±9.57	1002 ±13.27	1008 ±11.82	1012 ±9.82	852 ±10.28
Friability [%]	0.32 ±0.002	0.14 ±0.001	0.47 ±0.01	0.38 ±0.95	0.48 ±0.11	0.56 ±0.06	0.68 ±0.15	0.71 ±0.08	0.73 ±0.14	0.65 ±0.07
Drug content [%]	98.20 ±4.67	96.50 ±7.61	98.90 ±5.62	98.70 ±3.52	98.50 ±2.64	99.60 ±4.18	98.70 ±4.09	97.35 ±5.84	96.05 ±3.61	97.08 ±5.57

* The average of 10 determinations were given and the values are rounded off to a significant decimal.

sion equations of zero-order for formulations F_4, F_5 and F_7 (Fig. 2) revealed that the slope and regression coefficient (R^2) values for formulation F_7 were higher when compared to formulations F_4 and F_5 and the intercept value (constant) was less for formulation F_7 than for formulations F_4 and F_5. The x coefficient value was higher for formulation F_7. Based on these results, formulation F_7 was selected as the best. The regression graphs and equations of the zero-order release for F_4, F_5 and F_7 are shown in Fig. 2. These results indicate that formulation F_7 of the ciprofloxacin matrix tablets gave consistent release of ciprofloxacin up to 12 h.

The in vitro release of ciprofloxacin from the selected formulation (F_7) was analyzed for determination of the release kinetics. The data was processed into graphs to elucidate the linear relationship, i.e., kinetic principles. The regression analysis was done using Microsoft Excel statistical functions (Microsoft, Redmond, USA). The equations are given below:
Zero-order:

$$y = 8.1937\ t + 7.1653;\quad n = 12;\quad R^2 = 0.9847$$

First-order:

$$y = 0.0760 \log t + 1.215;\quad n = 12;\quad R^2 = 0.8606$$

As per the above equations, the release of ciprofloxacin hydrochloride followed zero-order kinetics, as the R^2 value was higher for zero-order than for first-order.

The release of ciprofloxacin from the matrix tablets was expected to be diffusion-rate-controlled. Hence, the data was processed as per the Higuchi equation. The regression equation for the data is given below:
Higuchi equation:

$$y = 37.936\ t^{1/2} + 32.043;\quad n = 12;\quad R^2 = 0.9901$$

The high R^2 value indicates that the release mechanism of ciprofloxacin from the matrix tablets was diffusion-controlled.

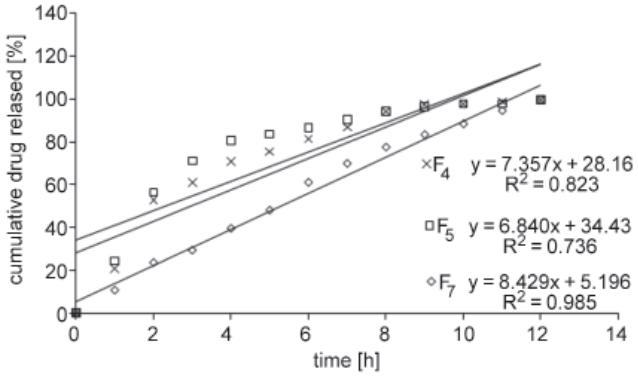

Fig. 2. Regression analysis of in vitro release data for the selected matrix tablets of ciprofloxacin hydrochloride (formulations F_4, F_5 and F_7)

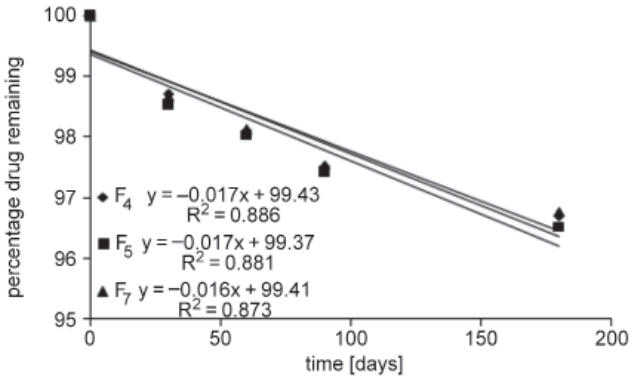

Fig. 3. Degradation profiles of ciprofloxacin hydrochloride tablets (formulations F_4, F_5 and F_7)

Stability studies on the matrix tablets (formulations F_4, F_5 and F_7) were carried out according to the ICH guidelines. Three tablets of each formulation were withdrawn, observed visually for physical appearance and analyzed for drug content at 0, 30th, 60th, 90th, and 180th day. All tablets retained physical integrity and no visual differences in color or texture were observed. The average drug content of the matrix tablets remaining at different intervals of time for each of the 3 formulations is shown in Table 4. From the data, shelf life (t90%) was calculated. The stability data from Table 4 (time vs % of drug remaining) for formulations F_4, F_5 and F_7 was processed into graphs using Microsoft Excel (Miscosoft, Redmond, USA) and regression equations were calculated for each formulation (Fig. 3). Degradation of ciprofloxacin followed first-order kinetics, as the regression coefficient value of the first-order plot was higher.

From the first-order plots, k values were calculated and substituted in the shelf life equation. The calculated values are given in Table 5. Percent drug content at 0 time and after 180 days was taken as C_0 and C (Table 5).

Table 4. Results of stability study of ciprofloxacin matrix tablets (formulations F_4, F_5 and F_7)

Time [days]	Quantity (mg/tablet)					
	F_4		F_5		F_7	
	[mg]	%	[mg]	%	[mg]	%
0	580	100	580	100	580	100
30	572.6	98.72	571.5	98.53	572.3	98.68
60	569.0	98.11	568.7	98.05	569.1	98.12
90	565.6	97.52	565.1	97.43	565.8	97.55
180	560.9	96.7	559.9	96.53	561.3	96.78

Table 5. Shelf life (t90%) of matrix tablet formulations of ciprofloxacin hydrochloride (formulations F_4, F_5 and F_7)

Formulation	$K \times 10^{-4}$	$t_{90\%}$ [days]
F4	1.861	565
F5	1.960	547
F7	1.821	555

The results of the stability study of the 3 formulations of ciprofloxacin matrix tablets revealed that these formulations are stable for a minimum period of 1.5 years. Analysis of the results gave significant observations, which were discussed in the light of current concepts and interrelationships among the other experimental results.

Conclusions

Ciprofloxacin hydrochloride-containing matrix tablets were prepared successfully. The tablets had good integrity and were stable for 18 months. Formulation F_7 gave a linear release pattern up to 12 h. The release of ciprofloxacin from formulation F_7 followed zero-order kinetics. The release mechanism was found to be diffusion-controlled as the Higuchi equation was obeyed.

References

1. Dash S, Murthy PN, Nath L, Chowdhury P. Kinetic modeling on drug release from controlled drug delivery systems. *Acta Pol Pharm*. 2010;67(3):217–223.
2. Raaijmakers JM, Vlami M, de Souza JT. Antibiotic production by bacterial biocontrol agents. *Antonie van Leeuwenhoek*. 2002;81(1-4):537–547.
3. Aminov R. History of antimicrobial drug discovery: Major classes and health impact. *Biochem Pharmacol*. 2017;133:4–19.
4. Stein GE. Pharmacokinetics and pharmacodynamics of newer fluoroquinolones. *Clin Infect Dis*. 1996;23:S19–S24.
5. Hassan Y, Alfadly SO, Azmin MN, et al. Bioequivalence evaluation of two different formulations of ciprofloxacin tablets in healthy volunteers. *Singapore Med J*. 2007;48(9):819–823.
6. Campoli-Richards DM, Monk JP, Price A, Benfield P, Todd PA, Ward A. Ciprofloxacin. A review of its antibacterial activity, pharmacokinetic properties and therapeutic use. *Drugs*. 1988;35(4):373–447.
7. Nicolle LE. Urinary tract infections in the elderly. *Clin Geriatr Med*. 2009;25:423–436.
8. Ball P. Ciprofloxacin: An overview of adverse experiences. *J Antimicrob Chemother*. 1986;18(Suppl D):187–193.
9. Segev S, Yaniv I, Haverstock D, Reinhart H. Safety of long-term therapy with ciprofloxacin: Data analysis of controlled clinical trials and review. *Clin Infect Dis*. 1999;28(2):299–308.
10. Bader MS, Hawboldt J, Brooks A. Management of complicated urinary tract infections in the era of antimicrobial resistance. *Postgrad Med*. 2010;122(6):7–15.
11. *United State Pharmacopeia 24 / National Formulary 19. Asian Edition*. Rockville, USA: USP Convention Inc; 2007.
12. Lachman L, Lieberman HA, Kanig JL. *Theory and Practice of Industrial Pharmacy*. 3rd ed. Bombay, India: Varghese Publishing House; 1990:297–299.
13. Sharma G, Pawar VK, Garg G, Awasthi R, Kulkarni GT. Taste masking of promethazine hydrochloride using Eudragit E100 via solid dispersion technique to develop fast disintegrating tablets. *Pharm Lett*. 2010;2(3):83–94.
14. Awasthi R, Kulkarni GT, Ramana MV, et al. Dual crosslinked alginate-pectin network as sustained release matrix for repaglinide. *Int J Biol Macromol*. 2017;97:721–732.
15. Ramana MV, Awasthi R, Ghisleni DDM, et al. Preparation and characterization of metoprolol tartrate containing matrix type transdermal drug delivery system. *Drug Deliv Transl Res*. 2017;7(1):66–76.

Polimery w Medycynie

Polymers in Medicine